Institute for Theoretical Physics
University of Cologne

Quantum Ratchets

Bachelorthesis
January 26, 2012

Under supervision of
Prof. Dr. Achim Rosch

Second Examiner
Priv.-Doz. Dr. Ralf Bulla

Submitted by Stefan Wolff
Matriculation number 4889274
Cologne 2011/2012

Abstract

In the present thesis we investigate the quantum dynamics of bosonic cold dilute atoms loaded in a one-dimensional optical lattice. A quantum ratchet effect has been obtained after breaking the spatiotemporal symmetries present in the system. This has been done via a time-periodic space-dependent hopping, the influence of an alternating oscillatory potential and introducing a phase shift among them both.

As a result an asymptotic unidirectional transport of particles is retrieved by means of numerical calculations using a Runge-Kutta method.

In the framework of Gross-Pitaevskii theory, we study the asymptotic current as a function of the driving frequency and use the Floquet theory to explain the eigenfrequencies within a perturbative limit. Additionally, the role of the time-reversal symmetry is quantified in terms of the relative phase shift .

Finally, leaving the limit of weak interactions and considering stronger strengths, the system dynamics reveals a sharp transition between a regular regime and a chaotic behaviour.

Zusammenfassung

In der vorliegenden Bachelorarbeit untersuchen wir die Quantendynamik von bosonischen kalten Atomen, die in einem eindimensionalen optischen Gitter gefangen sind. Es wurde nach der Brechung von örtlichen und zeitlichen Symmetrien des Systems ein Quanten-Ratchet-Effekt erreicht. Dies wurde über ein zeitlich periodisches Quanten-Hopping, ein oszillierendes alternierendes Potential und einen eingeführten Phasenunterschied zwischen beiden realisiert.

Als Ergebnis wurde ein gerichteter Transport von Teilchen mit Hilfe von numerischen Berechnungen in Form eines Runge-Kutta-Verfahrens erhalten.

Wir beschreiben den asymptotischen Strom weiter im Rahmen der Gross-Pitaevskii-Theorie als Funktion der treibenden Frequenz des Systems und benutzen die Floquet-Theorie um die Eigenfrequenzen im perturbativen Grenzfall zu erklären. Zusätzlich wird die Rolle der Zeit-Umkehr-Symmetrie in Bezug auf die Phasendifferenz quantifiziert.

Schliesslich verlassen wir den Bereich der schwachen Wechselwirkungen und betrachten starke Teilchen-Teilchen-Interaktionen. Dabei zeigt sich ein scharfer Übergang zwischen einem regulären Regime und einem chaotischen Verhalten.

Contents

List of Figures

1 Introduction

Cold atoms trapped in optical lattices offer a wide range of possibilities for both experimental and theoretical access to many-body quantum systems. The high degree of tunability of the lattice parameters, due to the relative arrangement of counter-propagating lasers, allows us to easily manipulate potential parameters in space and time. Moreover, the interaction strength between the trapped particles can be varied with the use of magnetically tunable Fleshbach resonances [1].

The unidirectional transport in absence of a bias force has been subject to many studies in the last decades. This is interesting both, in a classical as well as in a quantum consideration. For instance, thermal noise can evoke a directed motion by transcending potential barriers, which are known as Brownian motors [2]. The idea consists in generating work at a microscopic scale. This effect has also been used to describe molecular engines in asymmetric environments with non-Gaussian [3] as well as Gaussian noise[4]. In the present work we discuss Hamiltonian quantum ratchet effect, which lacks dissipative effects.

It has been shown, that in order to generate a finite asymptotic current the breaking of time-reversal symmetry in combination with a broken spatial symmetry is sufficient and essential [5]. Our goal is to maximize the outcoming current by systematic study of the system parameters.

Moreover, the role of interactions has captured the interest of the community. Contradictory studies have been published in the frame of non-interacting and weakly interacting systems [6][5]. Ref [6] states that a directed current occurs only if the interaction exceeds a critical value, while in ref [5] a finite net-transport of atoms can be retrieved even in the absence of interactions when the relevant symmetries are broken. Therefore, the use of interactions as a quantum analogon to Brownian motion in classical ratchets is still a very attractive topic.

The work on this thesis gave me the opportunity to become familiar with the use of numerical methods in the context of modern physical problems and also enabled me to gain experience with fundamental theoretical concepts, which are widely used in state-of-the-art research. That is an additional reasons why I consider it worth concentrating on quantum ratchets.

Since this thesis is based on a variety of theoretical ideas, we will give a short review of the central used elements in the following chapter.

1.1 Fundamentals of solid-state-physics

The purpose of the present thesis is to analyse the ratchet effect, presented by identical atoms loaded in a periodic optical lattice. We will start reviewing some fundamental principles of solid state physics. A lattice is defined as an infinite periodic array of discrete points [7], which in d dimensions is generated by a set of linear independent vectors $\vec{a}_1, \vec{a}_2, ..., \vec{a}_d$. A lattice point $\vec{R}$ can be reached by a linear combination of these base-vectors with integer coefficients $n_1, n_2, ..., n_d$,

$$\vec{R} = n_1\vec{a}_1 + n_2\vec{a}_2 + ... + n_d\vec{a}_d. \tag{1.1}$$

1.1.1 Bloch theory and band-structure

In a solid, the atoms are associated to the lattice points and the electrons are described as particles in the periodic potential formed by the atoms with periodicity $\vec{R}$, so that $V(\vec{r}) = V(\vec{r}+\vec{R})$. This spatial periodicity of the problem allows us to use Bloch's theorem

$$\psi_k(\vec{r}) = e^{i\vec{k}\vec{r}}u_k(\vec{r}), \qquad \text{where} \quad u_k(\vec{r}) = u_k(\vec{r}+\vec{R}). \tag{1.2}$$

The wave-functions $\psi_k(\vec{r})$ are referred to as Bloch waves. All wave vectors $\vec{k}$ can be reduced to the first Brillouin zone, so that the functions $\psi_{\vec{k}+\vec{G}_n}$ are solutions for the Schrödinger equation as well as $\psi_{\vec{k}}$. For this reason there exist multiple energy values for a given $\vec{k}$. The energy depends continuously from $\vec{k}$, so that there are diverse continuous functions $E_n(\vec{k})$ which are regarded as *bands*. As a convention the different possibilities are numbered with regard to their energies,

$$E(\vec{k}) = E_n(\vec{k}), \qquad E_1(\vec{k}) \leq E_2(\vec{k}) \leq ... . \tag{1.3}$$

In the case of a symmetric periodic potential $V(\vec{r}) = V(-\vec{r})$ the energy dependence on $\vec{k}$ is also symmetric. From this follows, that the propagation velocity $\partial_{\vec{k}}E(\vec{k})$ vanishes at the border of the Brillouin zone. Furthermore the energy-range of every band is limited to a certain interval. These different intervals are separated from each other by the so called gaps.

For the electrons in the lattice one can consider two cases. First the treatment of the electrons as quasi-free particles with the kinetic energy much greater than the potential ($\frac{\hbar^2k^2}{2m} \gg V$) and second the Tight-Binding-Approximation with the opposite property ($\frac{\hbar^2k^2}{2m} \ll V$) as shown in figure (1.1). The latter is suitable to study in the present work,

therefore this topic is explained in more detail in section (1.1.2).

1.1.2 Tight-binding model and Wannier-function

Since the kinetic energy of the electrons is much lower than the confining potential, a Bloch wave which describes quasi-free particles, is not longer appropriate[8]. Instead, a

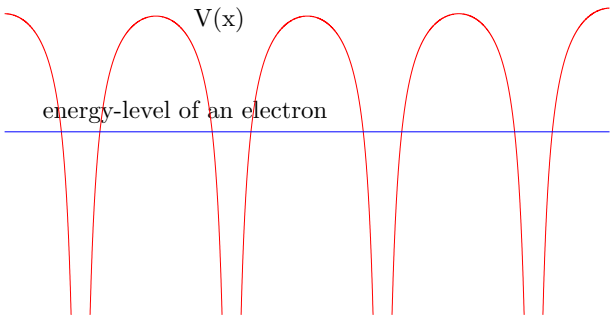

Figure 1.1: Tight-binding approximation for $\frac{\hbar^2 k^2}{2m} \ll V$

more suitable way is, to consider the electrons as bounded to the atoms or the lattice points, so that their wave-function is associated with the atomic function. For this purpose the well localized Wannier functions are widely used. They are constructed by a linear combination of Bloch functions and form an orthonormalized set

$$w_j(\vec{r} - \vec{R}_j) = \frac{1}{\sqrt{N}} \sum_k e^{-i\vec{k}\vec{R}_j} \psi_{\vec{k}}(\vec{r}). \tag{1.4}$$

1.2 Floquet theory

The Floquet theory is the analogous to the Bloch theory to study periodically time-dependent systems. The main advantage is that it allows us to transform the original time-periodic system to a time-independent one, where it is needed to solve an eigenvalue problem. Hence the Floquet theory is very important in the study of dynamical systems in the present thesis it is used to explain the eigenfrequencies of the ratchet system.

The Bloch theorem, as it was already introduced, states that the wave function of a system in a periodic potential may be written as superposition of plane waves modulated by a function $u_k(\vec{r})$ (eq. 1.2) that has the same period as the potential. The same underlying

ideas have been introduced in the context of time-periodic problems by Floquet (1883). As a result there is a common language among these two theories.

The starting point is the time-dependent Schrödinger equation with periodic Hamiltonian $\hat{H}(t) = \hat{H}(t+T)$ [9]. To express the wave function $|\psi(t)\rangle$ the Floquet theorem

$$|\psi(t)\rangle = e^{-i\epsilon_\alpha t}|\phi_\alpha(t)\rangle, \qquad \text{where} \qquad |\phi_\alpha(t)\rangle = |\phi_\alpha(t+T)\rangle, \tag{1.5}$$

is used. Arranging the terms one has [10]

$$\begin{aligned} 0 &= \left(\hat{H}(t) - i\partial_t\right) e^{-i\epsilon_\alpha t}|\phi_\alpha(t)\rangle \\ &= e^{-i\epsilon t}\hat{H}(t)|\phi_\alpha(t)\rangle - i\left[-i\epsilon_\alpha e^{-i\epsilon_\alpha t}|\phi_\alpha(t)\rangle + e^{-i\epsilon_\alpha t}\partial_t|\phi_\alpha(t)\rangle\right] \\ \Longrightarrow \epsilon_\alpha|\phi_\alpha(t)\rangle &= \underbrace{\left(\hat{H}(t) - i\partial_t\right)}_{\equiv\hat{\mathcal{H}}_F}|\phi_\alpha(t)\rangle. \end{aligned} \tag{1.6}$$

The operator $\hat{\mathcal{H}}_F$ is denoted as the Floquet Hamiltonian, its eigenvalues are the so called quasi-energies ϵ_α and its eigenvectors are the Floquet states $|\phi_\alpha(t)\rangle$ which form a complete basis. A Fourier-transformation gives of the time-dependent Floquet states gives

$$|\phi_\alpha(t)\rangle = \sum_n e^{-in\omega t}|\phi_{\alpha,n}\rangle. \tag{1.7}$$

Plugging this into equation (1.6) leads to a shift for the quasi energy

$$(\epsilon_\alpha + n\omega)|\phi_{\alpha,n}\rangle = \sum_m \left(\mathcal{H}_F\right)_{nm}|\phi_{\alpha,m}\rangle. \tag{1.8}$$

The time-evolution operator

$$\hat{U}(t) = e^{-i\int \hat{H}dt} \tag{1.9}$$

can be expressed, as a function of the Floquet Hamiltonian $\hat{\mathcal{H}}_F$ instead of $\hat{H}$, therefore the Floquet states $|\phi\rangle$ diagonalize $U(t)$ with eigenvalues $e^{-i\epsilon_\alpha t}$.

Finally the time-evolved state $|\psi(t)\rangle$ can be computed by

$$\begin{aligned} |\psi(t)\rangle = \hat{U}(t)|\psi(0)\rangle &= \hat{U}(t)\sum_\alpha |\phi_\alpha(t)\rangle \underbrace{\langle\phi_\alpha(t)|\psi(0)\rangle}_{\equiv u_{\alpha,0}} = \sum_\alpha u_{\alpha,0}e^{-i\epsilon_\alpha t}|\phi_\alpha(t)\rangle \\ &= \sum_\alpha e^{-i\epsilon_\alpha t}\sum_n u_{\alpha,0}e^{-in\omega t}|\phi_{\alpha,n}\rangle. \end{aligned} \tag{1.10}$$

For this reason it is equivalent to solve the time-dependent Schrödinger equation. The difficulty in this eigensystem is implied by its dimension because the index n in equation (1.10) runs from $-\infty$ to ∞, so that the eigensystem is infinite. To reduce the time-independent basis $\{\phi_\alpha\}$ the concept of a Floquet-Brillouin zone must be introduced [11]. Nevertheless the Floquet approach is very useful and gives in our application a good addition to our numerical results.

1.3 Cold atoms

One of the milestones of modern physics was the possibility to cool atoms down to temperatures close to the absolute zero point of 0K. The process involves several experimental cooling and trapping techniques like Laser-cooling [12] or evaporative cooling [13], for which Cohen-Tannoudji, Phillips and Chu were awarded with the nobel prize in 1997.
At this very low temperatures the quantum properties of the atoms prevail over the classical character. The DeBroglie wavelength is very long, so that it reaches the order of the interatomic distance and the system can reach the quantum degenerate state which for bosons is known as the Bose-Einstein condensation (BEC)[13]. Due to the big impact of the BEC achievement, Ketterle, Cornell and Wieman received the nobel prize in 2001.

1.3.1 Optical lattices

An optical lattice consists of two counter-propagating laser beams, which create a standing wave with spatially fixed intensity maxima and minima. There are two possible ways of laser field-particle interaction: First via a dissipative force, which arises from the momentum transfer in the absorption and emission of photons by the atoms[14]. This is the basic effect in the laser cooling technique. Secondly via a conservative force, which is originated by the atomic dipole moment induced by the laser field [14], being the basis for the creation of an optical lattice. To guarantee that only conservative processes are involved the lattice is ramped up after the cooling process and the laser frequency needs to be highly detuned from the transition frequency of the trapped atoms. The dipole moment of the atoms, induced by the electric field is defined over the polarisability α,

$$\vec{d} = \alpha(\omega)\vec{E}, \qquad \text{where } \omega \text{ is the laser frequency.} \tag{1.11}$$

Since the intensity is proportional to the electric field $I \propto |E|^2$, the dipole potential is given by

$$V_{dipole} = -\frac{1}{2}\langle \vec{d}\vec{E}(\vec{r})\rangle \quad \propto \quad \Re(\alpha) I(\vec{r}). \tag{1.12}$$

Considered the dependency of the decay rate Γ and the frequency difference $\Delta = \omega - \omega_0$, where ω_0 is the transition frequency, the dipole potential is rewritten as

$$V_{dipole} \propto \frac{\Gamma}{\Delta} I. \tag{1.13}$$

So, depending on the direction of the detuning, the potential in the optical lattice is repulsive ($V > 0, \omega \gg \omega_0$) or attractive ($V < 0, \omega \ll \omega_0$). Furthermore spatial and temporal potentials can be created by modulation of the intensity of the laser beam. For instance a potential of the form $V(x) = V_0 \sin(kx)$, producing a one-dimensional lattice, can be generated. In practise this is done with a spatial limitation of the laser beam in y- and z-direction by two more lasers with gaussian intensity profile, perpendicular to the first one and to each other [15][14]. The Gaussian profile can be approximated as harmonic up to second order

$$V(x) = V_0 \sin^2(kx) + \frac{1}{2}(\omega_y^2 y^2 + \omega_z^2 z^2). \tag{1.14}$$

Higher dimensional lattices can be realized by a modulation of the lasers in y- and z-direction. A two-dimensional example is shown in figure (1.2). The great advantage of

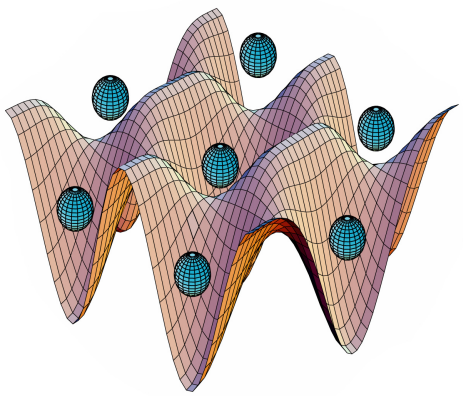

Figure 1.2: Optical lattice in 2 dimensions (Source: [16])

optical lattices is that the parameters of the system, like potential depth, lattice geometry and interatomic interaction strengths [17] are highly tunable, opening a new field for theoretical and experimental investigations.

1.4 Many-body-Schrödinger-equation

Since we are interested in the time evolution of a many-body system, we use the Schrödinger equation to model the problem. More precisely we are dealing with an ensemble of N indistinguishable non-relativistic weakly interacting bosons. The Hamiltonian of the system is of the form

$$\hat{\mathcal{H}} = \sum_{i=1}^{N} \hat{T}_i + \sum_{i=1}^{N} \hat{V}_i + \frac{1}{2} \sum_{\substack{i,j=1 \\ i \neq j}}^{N} \hat{U}_{ij}, \tag{1.15}$$

where $\hat{T}_i$ is the kinetic energy, $\hat{V}_i$ the external trapping potential and $\hat{U}_{ij}$ the interaction. The indices i and j denote the lattice position of the particles. We make use of the theoretical concept of second quantisation, which simplifies the formulation of the problem enormously and allows us to describe a many-body system in a transparent way in contrast to the first quantisation formulation. Due to the complexity of the problem, it is necessary to solve the problem numerically. The details about the numerical methods used in this thesis are illustrated in Chapter 2.

1.4.1 Second quantisation

The derivation and statements in this section are mainly following the description in [18] and [19].

The formalism of second quantisation [18] is based on the creation and annihilation operators $\hat{b}^\dagger$ and $\hat{b}$ respectively in the linear harmonic oscillator. These two operators act on a Hilbert space of states which here are expressed in the basis of the occupation number states or Fock states. The Fockspace $\mathscr{H}$ is defined as the direct sum of the Hilbert spaces $\mathscr{H}_N$ [19] with a given number N of particles,

$$\mathscr{H} = \mathscr{H}_0 \oplus \mathscr{H}_1 \oplus \ldots \oplus \mathscr{H}_i \oplus \ldots = \bigoplus_{N=0}^{\infty} \mathscr{H}_N \ . \tag{1.16}$$

This allows us to examine systems with fluctuating total number of particles. A suitable and useful representation is given by the Basis $\mathbb{B}$ with the non-negative integers n_i which mark the occupation of the i^{th} state and are eigenvalues of the so called number operator $\hat{n}_i$,

$$\mathbb{B} = \{|n_1, n_2, \ldots, n_i, \ldots\rangle\}. \tag{1.17}$$

The numbers n_i can take every arbitrary non-negative integer value for bosons and because

of the Pauli exclusion principle either 0 or 1 for fermions. Henceforth we concentrate exclusively on the bosonic case. The definition of the number operator is done in terms of the above mentioned creation and annihilation operators. The operator $\hat{b}_i$ annihilates a particle in state i, while $\hat{b}_i^\dagger$, which is the Hermitian conjugate of $\hat{b}_i$, creates a particle in the state i. So in case of $n_i \neq 0$,

$$\hat{b}_i|n_1, n_2, \ldots, n_i, \ldots\rangle \propto |n_1, n_2, \ldots, n_i - 1, \ldots\rangle, \tag{1.18}$$

$$\hat{b}_i^\dagger|n_1, n_2, \ldots, n_i, \ldots\rangle \propto |n_1, n_2, \ldots, n_i + 1, \ldots\rangle. \tag{1.19}$$

The number operator is then defined by $\hat{n}_i \equiv \hat{b}_i^\dagger \hat{b}_i$ and fulfils for bosons the commutator relations

$$[b_i, b_j^\dagger] = \delta_{ij}\mathbb{1}, \quad [b_i, b_j] = [b_i^\dagger, b_j^\dagger] = 0, \quad [\hat{n}_i, \hat{b}_i] = -\hat{b}_i, \quad [\hat{n}_i, \hat{b}_i^\dagger] = \hat{b}_i^\dagger. \tag{1.20}$$

So the normalisation of the states $\hat{b}_i|n_1, n_2, \ldots, n_i, \ldots\rangle$ and $\hat{b}_i^\dagger|n_1, n_2, \ldots, n_i, \ldots\rangle$ leads to the following equalities for the bosonic creation and annihilation operators

$$\hat{b}_i|n_1, n_2, \ldots, n_i, \ldots\rangle = \sqrt{n_i}\,|n_1, n_2, \ldots, n_i - 1, \ldots\rangle, \tag{1.21}$$

$$\hat{b}_i^\dagger|n_1, n_2, \ldots, n_i, \ldots\rangle = \sqrt{n_i + 1}\,|n_1, n_2, \ldots, n_i + 1, \ldots\rangle. \tag{1.22}$$

The criterion of the normability of $\hat{b}_i|\psi\rangle$ is satisfied for a normalised state $|\psi\rangle$ if the absolute value $\langle\psi|\hat{b}_i^\dagger\hat{b}_i|\psi\rangle = n_i$ is greater or equal to zero. As a result of that the lowest possible value for n_i so that $\hat{b}_i|\psi\rangle \in \mathscr{H}$ is 0,

$$n_i \in \{0, 1, 2, \ldots\}. \tag{1.23}$$

1.4.2 Operators in second quantisation

In a many-body problem it is possibly to describe the total state $|\psi\rangle$ of the system by a direct product of one-particle states $|\psi_i\rangle$. A given operator $\hat{A}$ which acts on the j^{th} particle can be expressed by

$$\hat{A}|\psi\rangle = |\psi_1\rangle \otimes \ldots \otimes \hat{A}^{(j)}|\psi_j\rangle \otimes \ldots |\psi_N\rangle \tag{1.24}$$

1.4.3 Time-evolution of field-operators (Heisenberg picture)

For instance considering the operator $\hat{A}^{(j)} = |\alpha\rangle\langle\beta|$, the result of applying it on the state $|\psi\rangle$ is given by

$$\hat{A}|\psi\rangle = |\psi_1\rangle o \times \ldots \otimes |\psi_{j-1}\rangle \otimes |\alpha\rangle \otimes \ldots |\psi_N\rangle\langle\beta|\psi_j\rangle. \tag{1.25}$$

This technique already looks very similar to the concept of second quantisation. In fact the operator $\hat{A}$ can be rewritten by using ladder operators, creating a particles $\hat{b}_\alpha|vac\rangle = |\alpha\rangle$ in the vacuum and annihilating a particle in dependence of β so that $\hat{A} = \hat{b}^\dagger_\alpha \hat{b}_\beta$. With this property and the use of the completeness relation of the basis $\{|\alpha\rangle\}$ and $\{|\beta\rangle\}$ the operator is expressed by [19]

$$\hat{A}^{(j)} = \sum_{\alpha,\beta} |\alpha\rangle\langle\alpha|A^{(j)}|\beta\rangle\langle\beta| \longrightarrow \hat{A} = \sum_{\alpha,\beta} \hat{b}^\dagger_\alpha \langle\alpha|A|\beta\rangle \hat{b}_\beta. \tag{1.26}$$

An operator that involves more than one-particle operators, like an operator describing an interaction between two particles can be represented as followed,

$$\hat{B} = \frac{1}{2} \sum_{\alpha,\beta,\alpha',\beta'} \hat{b}^\dagger_{\alpha'} b^\dagger_{\beta'} \langle\alpha,\beta|B|\alpha,\beta\rangle \hat{b}_\alpha \hat{b}_\beta. \tag{1.27}$$

1.4.3 Time-evolution of field-operators (Heisenberg picture)

We introduce the field operators as a linear combination of the ladder operators as follows,

$$\hat{\psi}(\vec{r}) = \sum_i \psi_i(\vec{r}) \hat{b}_i, \tag{1.28}$$

$$\hat{\psi}^\dagger(\vec{r}) = \sum_i \psi_i(\vec{r}) \hat{b}^\dagger_i, \tag{1.29}$$

where the coefficients $\psi_i(\vec{r})$ are the single particle wave functions for the quantum number i and the summation goes over the complete associated set of states. The field operators also satisfy the commutator relations

$$\left[\hat{\psi}(\vec{r}), \hat{\psi}^\dagger(\vec{r}\,')\right] = \delta(\vec{r} - \vec{r}\,'), \qquad \left[\hat{\psi}(\vec{r}), \hat{\psi}(\vec{r}\,')\right] = \left[\hat{\psi}^\dagger(\vec{r}), \hat{\psi}^\dagger(\vec{r}\,')\right] = 0. \tag{1.30}$$

The time evolution can be calculated for any arbitrary operator $\hat{A}$ in the Heisenberg image with $i\frac{d}{dt}\hat{A} = \left[\hat{A}, \hat{\mathcal{H}}\right]$, so that

$$i\frac{d}{dt}\hat{\psi} = \left[\hat{\psi}, \hat{\mathcal{H}}\right]. \tag{1.31}$$

Now the motivation for the development of second quantisation becomes obvious, since it is possible to express the Hamiltonian by the use of field operators in an convenient and intuitive way,

$$\hat{\mathcal{H}} = \int d\vec{r}\, \hat{\psi}^\dagger(\vec{r}) \underbrace{\left[-\frac{\hbar^2}{2m}\nabla^2 + V_{ext}(\vec{r})\right]}_{\equiv \hat{\mathcal{H}}_0} \hat{\psi}(\vec{r}) + \frac{1}{2}\int d\vec{r}d\vec{r}'\, \hat{\psi}^\dagger(\vec{r})\, \hat{\psi}^\dagger(\vec{r}')U(\vec{r}-\vec{r}')\, \hat{\psi}(\vec{r})\, \hat{\psi}(\vec{r}'). \tag{1.32}$$

1.5 Gross-Pitaevskii theory

1.5.1 Statistical ensembles

The content of this chapter was mainly written with reference to the presentation in Landau and Lifschitz in [20].

There are several ways to analyse a many-particle system, depending on the conservation or not-conservation of the extensive quantities. In the case of a monoatomic gas the extensive quantities are given by the internal energy U, the Volume V of the system and the total number of particles N. For this set-up there are three common ensembles [20], called canonical ensembles. The first one is the *micro-canonical ensemble*. This describes a closed system where all the extensive quantities U,V and N are conserved. Especially the energy $H_{V,N}$ of the micro-states x is fixed. An ensemble, in which the energy fluctuates but the particle number and the volume are still constant, is referred to as the *canonical ensemble*. In the partition function of this ensemble every micro-state x is weighted with the Boltzmann factor, containing the inverse temperature $\beta = (k_B T)^{-1}$

$$Z_C = \int dx e^{-\beta H_{V,N}(x)}. \tag{1.33}$$

The last ensemble, the *grand-canonical ensemble*, additionally allows the exchange of particles with an external particle reservoir, while the volume is still kept constant. Because N is a discrete number the partition is expanded with a sum over all N, with the intensive parameter $\mu = \partial_N U$, known as the chemical potential, belonging to the extensive quantity N

$$Z_{GC} = \sum_{N=0}^{\infty} e^{-\beta\mu N} Z_C. \tag{1.34}$$

The grand-canonical ensemble is very useful in the context of many-body quantum systems

like a Bose-Einstein condensation, where the occupation number of different states varies due to quantum and/or thermal fluctuations. For this reason we use the grand-canonical ensemble in our later considerations.

1.5.2 Bose-Einstein-condensation

As the later examined systems models a Bose-Einstein condensate of cold atoms trapped in an optical lattice, we will briefly mention a few characteristics of this state of matter.

The main feature of a Bose-Einstein Condensate (BEC) is, that below a certain critical temperature T_C, a macroscopic number of particles occupies the ground state of the system. Because of the Pauli exclusion principle this is achievable only for bosons. The high occupation of one quantum state generates a single wave function which can extend macroscopically in the order of a few millimetres [21]. That is a reason why a Bose-Einstein condensate is a perfect environment to experiment with quantum phenomena.

At first it is useful to investigate the one-body density matrix [22] $n^{(1)}(\vec{r},\vec{r}\,')$ defined by

$$n^{(1)}(\vec{r},\vec{r}\,') = \langle\hat{\psi}^\dagger(\vec{r})\hat{\psi}(\vec{r}\,')\rangle. \tag{1.35}$$

The density matrix is Hermitian, why there exists a basis of single particle functions in which $n^{(1)}(\vec{r},\vec{r}\,')$ is diagonal,

$$n^{(1)}(\vec{r},\vec{r}\,') = \sum_i n_i\varphi_i^*(\vec{r})\varphi_i(\vec{r}\,') = N_0\varphi_0^*(\vec{r})\varphi_0(\vec{r}\,') + \sum_{i\neq 0} n_i\varphi_i^*(\vec{r})\varphi_i(\vec{r}\,'). \tag{1.36}$$

As mentioned above, a system undergoes to a BEC if the lowest energy state $\varphi_0(\vec{r})$ is macroscopically occupied. The diagonal elements ($\vec{r}=\vec{r}\,'$) of this matrix give us information about the number of bosons in the i^{th} state. The off-diagonal elements ($\vec{r}\neq\vec{r}\,'$) carry information of the momentum distribution of the particles.

The ideal non-interacting Bose gas which will be considered in Chapter 3 in the canonical ensemble, has a average occupation of the i^{th} state [22] given by the Bose-Einstein distribution

$$\overline{n}_i = \frac{1}{\exp[\beta(E_i-\mu)]-1} \quad . \tag{1.37}$$

For all configurations of $\overline{n}_i$ the normalisation condition $\sum_i \overline{n}_i = N$ must be fulfilled. The chemical potential depends on the temperature because for increasing temperature also the chemical potential rises. Let $\overline{n}_0$ be the lowest energy state. The energy states E_i are

independent of the temperature.Then, depending on the density of states of the E_i there can exist a critical temperature T_C, where μ approaches E_0, and the fraction of condensed particles $\overline{n}_0$ becomes macroscopic.

1.5.3 Mean-field-approximation

In the present work we are also interested in studying the role of interactions in the bosonic lattice gas. A good starting-point to study weakly interacting particles is using a mean field approach for the field operator. This approximation has been applied successfully to describe several BEC properties [23][13][17]. The main idea is to split up the field operator in the macroscopically occupied condensed fraction and a perturbation containing the non-condensed particles [23]

$$\hat{\psi}(\vec{r}) = \hat{\psi}(\vec{r}) + \delta\hat{\psi}(\vec{r}). \tag{1.38}$$

Since the fraction of the condensate $\overline{n}_0 = \frac{N_0}{N}$ is finite, one can assume that $N_0 \pm 1 \simeq N_0$ and the corresponding physical states do not change. As a consequence of that one can describe the system using coherent states and replace the operators $b_i^\dagger$ and $b_i^\dagger$ by their eigenvalues $\sqrt{N}$. Hence, the mean value of field operator $\langle\hat{\psi}(\vec{r})\rangle$ can be associated directly to the expectation values of the condensate fraction. This we are allows to change from operators to complex functions

$$\hat{\psi} \longrightarrow \psi \tag{1.39}$$

This complex function is defined as the order parameter and also known as the condensate wave function. In fact the many-body problem is treated in this approach as a one-body problem in presence of an external mean field.

1.5.4 s-wave-scattering

We are considering a dilute and cold gas of bosonic atoms. When these slow particles scatter each other, they cannot resolve their internal structure since their De Broglie wavelength is very long. Therefore, the details of the interacting potential $U(\vec{r}-\vec{r}')$ are not important, but only how the potential behaves at long length scales. The formal way to solve the problem would be to do a partial wave expansion using the angular momentum components of the outgoing particles. At low energies the most relevant term is the lowest order which is the spherical symmetric (angular momentum $l = 0$) outgoing wave. This is the so called s-wave scattering.

Since the particles do not realize their structure, the interacting potential can be replaced by a delta potential in the Gross-Pitaevskii theory within the mean-field equation discussed below

$$U(\vec{r}-\vec{r}') = g\delta(\vec{r}-\vec{r}'), \qquad \text{where} \quad g = \frac{4\pi\hbar^2 a}{m}. \tag{1.40}$$

The constant g is proportional to the s-wave scattering length a, which depends on the atomic properties. In experiments, alkali atoms are used because of the filled up shells and the single electron in the s-orbital, holding the choice of the δ-potential.

1.5.5 Gross-Pitaevskii equation

The above mentioned properties of a dilute, weak interacting, cold gas of atoms converge in the Gross-Pitaevskii equation (GPE). The starting point for the GPE is the Heisenberg equation for the evolution of the field operators. The commutator of equation (1.31) with the Hamiltonian of equation (1.32) has the form

$$\left[\hat{\psi}(\vec{r},t), \int d\vec{r}'\ \hat{\psi}^\dagger(\vec{r}')\ \hat{\mathcal{H}}_0\ \hat{\psi}(\vec{r}')\ + \frac{1}{2}\int d\vec{r}'d\vec{r}''\ \hat{\psi}^\dagger(\vec{r}')\ \hat{\psi}^\dagger(\vec{r}'')U(\vec{r}'-\vec{r}'')\ \hat{\psi}(\vec{r}')\ \hat{\psi}(\vec{r}'').\right]$$

where

$$\hat{\mathcal{H}}_0 = \hat{T}(\vec{r}') + \hat{V}(\vec{r}') \tag{1.41}$$

Using the commutator relations(1.30) we obtain the time evolution of the quantum state $\hat{\psi}(\vec{r},t)$ by

$$\begin{aligned} i\hbar\partial_t\hat{\psi}(\vec{r},t) &= \int d\vec{r}'\ \delta(\vec{r}-\vec{r}')\ \hat{\mathcal{H}}_0\ \hat{\psi}(\vec{r}')\ + \frac{1}{2}\int d\vec{r}'d\vec{r}''\ \delta(\vec{r}-\vec{r}')\ \hat{\psi}^\dagger(\vec{r}'')U(\vec{r}'-\vec{r}''')\ \hat{\psi}(\vec{r}')\ \hat{\psi}(\vec{r}'') \\ &= \left[\hat{\mathcal{H}}_0 + \int d\vec{r}'\hat{\psi}^\dagger(\vec{r}')U(\vec{r}-\vec{r}')\hat{\psi}(\vec{r}')\right]\hat{\psi}(\vec{r},t). \end{aligned} \tag{1.42}$$

The next step is to do the mean-field approach (1.38) in the sense that the field operators are identified by complex functions i.e. $\hat{\psi} \to \psi$ and $\hat{\psi}^\dagger \to \psi^*$. So all operators are now changed to complex functions. Finally, the interaction potential is substituted by the δ-potential (1.40) and equation (1.42) is rewritten as

$$i\hbar\partial_t\psi(\vec{r},t) = \left[-\frac{\hbar^2}{2m}\nabla^2 + V(\vec{r},t) + g\left|\psi(\vec{r},t)\right|^2\right]\psi(\vec{r},t)\,. \tag{1.43}$$

This is known as the Gross-Pitaevskii equation (GPE) and is a common starting point to study weakly interacting bosonic gases which are considered throughout the present work.

In particular in this thesis the GPE is used to analyse the quantum ratchet effect of the particles in a one-dimensional lattice under certain conditions. We consider our system to be in the tight-binding regime, mentioned in section (1.1.2). In that context the Bose-Hubbard model is introduced now.

1.6 Bose-Hubbard model

The concept of the Bose-Hubbard model has mainly been worked out with the help of [24] and [25].

In this thesis we focus on a one-dimensional problem. This is experimentally realizable with an optical lattice with a modulated potential in one direction and a translation-invariant potential in the other two.
In the tight binding approach particles are fixed to one site and can solely jump to an adjacent site, as it is sketched in figure (1.3). More precisely the Wannier functions of the

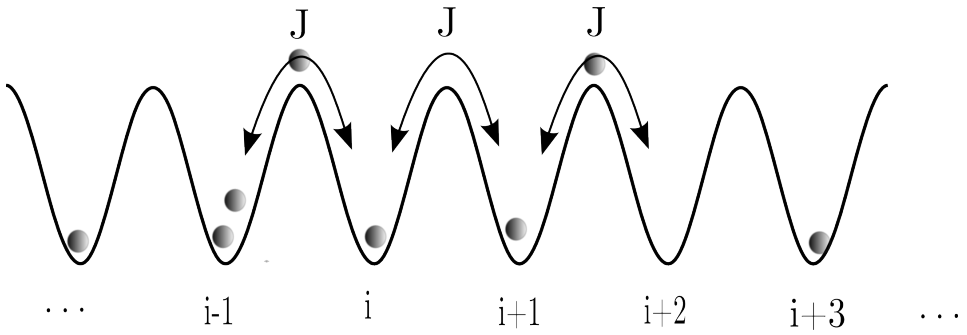

Figure 1.3: System with equal hopping parameters $J_{ij} = J$

atoms are separated by comparative high potential barriers. As a result, the behaviour of atoms confined in an optical lattice can be described by the creation and annihilation operators $\hat{b}_i^\dagger$ and $\hat{b}_i$, where i marks the lattice sites. The idea of the Bose-Hubbard model is to express the Hamiltonian (1.32) in terms of the ladder operators. Therefore we replace the field operators in the Hamiltonian (1.32) with the expressions in equation (1.29), where the wave functions can be described by Wannier functions (1.4 because of the high locality of the atoms,). Consequently the Hamiltonian can be rewritten, using the δ-potential

from the s-wave scattering, as

$$\begin{aligned}\hat{\mathcal{H}} &= \sum_{i,j} \int d\vec{r} \hat{b}_i^\dagger w^*(\vec{r}-\vec{R}_i) \left[-\frac{\hbar^2}{2m}\nabla^2 + V_{ext}(\vec{r})\right] \hat{b}_j w(\vec{r}-\vec{R}_j) \\ &\quad + \frac{1}{2}U \sum_{i,j,k,l} \int d\vec{r} \hat{b}_i^\dagger w^*(\vec{r}-\vec{R}_i) \hat{b}_j^\dagger w^*(\vec{r}-\vec{R}_j) \hat{b}_k w(\vec{r}-\vec{R}_k) \hat{b}_l w(\vec{r}-\vec{R}_l) \\ &= \sum_{\langle i,j\rangle} -J_{i,j} \hat{b}_i^\dagger \hat{b}_j + \sum_i V_i \hat{b}_i^\dagger \hat{b}_i + \frac{1}{2}\sum_i U_i \hat{b}_i^\dagger \hat{b}_i^\dagger \hat{b}_i \hat{b}_i. \end{aligned} \tag{1.44}$$

The last step takes the limitation for the hopping to the adjacent sites and the negligence of interaction between atoms in different sites into account. The notation $\langle i,j\rangle$ represents the set of all neighbouring sites i and j. The factors $J_{i,j}$, V_i and U_i are the matrix-elements given by

$$\begin{aligned} J_{i,j} &= -\int d\vec{r} w^*(\vec{r}-\vec{R}_i) \left[-\frac{\hbar^2}{2m}\nabla^2 + V_{ext}(\vec{r})\right] w(\vec{r}-\vec{R}_j)\,, \\ V_i &= \int d\vec{r} w^*(\vec{r}-\vec{R}_i) \left[-\frac{\hbar^2}{2m}\nabla^2 + V_{ext}(\vec{r})\right] w(\vec{r}-\vec{R}_i)\,, \\ U_i &= 2g \int d\vec{r} \left|w(\vec{r}-\vec{R}_i)\right|^4\,. \end{aligned} \tag{1.45}$$

In particular $J_{i,j}$ is the probability for a particle to jump from i to j and is referred to as the hopping-parameter or simply the hopping. Following we will calculate the time-evolution of the field operator for one site using the Heisenberg-equation (1.31) and the ladder operators are replaced by the corresponding field operators. We obtain for the hopping part with the bosonic commutation (1.30) relations

$$\begin{aligned} i\partial_t \hat{\psi}_k &= [\hat{\psi}_k, \sum_{\langle i,j\rangle} -J_{i,j} \hat{\psi}_i^\dagger \hat{\psi}_j] = \sum_{\langle i,j\rangle} -J_{i,j} \left(\hat{\psi}_k \hat{\psi}_i^\dagger \hat{\psi}_j - \hat{\psi}_i^\dagger \hat{\psi}_j \hat{\psi}_k\right) = \sum_{\langle i,j\rangle} -J_{i,j}\delta_{k,i}\hat{\psi}_j \\ &= -J\left(\hat{\psi}_{k+1} + \hat{\psi}_{k-1}\right). \end{aligned} \tag{1.46}$$

An analogous calculation is done for the potential

$$i\partial_t \hat{\psi}_k = [\hat{\psi}_k, \sum_i V_i \hat{\psi}_i^\dagger \hat{\psi}_i] = \sum_i V_i \left(\hat{\psi}_k \hat{\psi}_i^\dagger \hat{\psi}_i - \hat{\psi}_i^\dagger \hat{\psi}_i \hat{\psi}_k\right) = \sum_i V_i \delta_{i,k} \hat{\psi}_i = V_k \hat{\psi}_k, \tag{1.47}$$

and the interaction term

$$\begin{aligned} i\partial_t\hat{\psi}_k &= [\hat{\psi}_k, \sum_i \frac{U_i}{2}\hat{\psi}_i^\dagger\hat{\psi}_i^\dagger\hat{\psi}_i\hat{\psi}_i] = \sum_i \frac{U_i}{2}\left(\hat{\psi}_k\hat{\psi}_i^\dagger\hat{\psi}_i^\dagger\hat{\psi}_i\hat{\psi}_i - \hat{\psi}_i^\dagger\hat{\psi}_i^\dagger\hat{\psi}_i\hat{\psi}_i\hat{\psi}_k\right) \\ &= \sum_i \frac{U_i}{2}\left[\hat{\psi}_k, \hat{\psi}_i^\dagger\hat{\psi}_i^\dagger\right]\hat{\psi}_i\hat{\psi}_i = \sum_i \frac{U_i}{2}\left(\left[\hat{\psi}_k, \hat{\psi}_i\right]\hat{\psi}_i^\dagger + \hat{\psi}_i^\dagger\left[\hat{\psi}_k, \hat{\psi}_i\right]\right)\hat{\psi}_i\hat{\psi}_i \\ &= U_k\hat{\psi}_k^\dagger\hat{\psi}_k\hat{\psi}_k \quad . \end{aligned} \tag{1.48}$$

All terms considered, the time-dependence for a field operator of site i is then

$$i\partial_t\hat{\psi}_i = -J\left(\hat{\psi}_{i+1} + \hat{\psi}_{i-1}\right) + V_i\hat{\psi}_i + U_i\hat{\psi}_i^\dagger\hat{\psi}_i\hat{\psi}_i \quad . \tag{1.49}$$

The mean field approximation allows us the transfer $\hat{\psi} \to \psi$ and respectively $\hat{\psi}^\dagger \to \psi^*$. As a convention for a weak-interacting case U is replaced by g. The time-dependent mean field equation for the Bose-Hubbard model can be viewed as a discretized version of the GPE

$$i\partial_t\psi_i = -J(\psi_{i-1} + \psi_{i+1}) + V_i\psi_i + g|\psi_i|^2\psi_i. \tag{1.50}$$

1.7 Ratchet effect

In general context, the concept of ratchets refers to periodic systems with broken symmetries that present an unidirectional transport of particles in the presence of zero-averaged forces [26]. The involved symmetries are on the one hand of spatial and on the other hand temporal nature, and arise from the periodicity in space and time

$$x \to x + a \qquad \text{a: spatial period}\,, \tag{1.51}$$

$$t \to t + T \qquad \text{T: time period}\,. \tag{1.52}$$

An example of a classical ratchet is given in figure (1.4). In this case the ratchet effect results of a driving potential in a sawtooth-shape, that is switched on and off periodically. With the potential being switched on, the particles are trapped in the potential minima, so that they are well-localized. Then, in the absence of a potential,the particles disperse freely, owing to Brownian motion. If the potential is switched on again, some of the particles have moved over the potential spike and feel a attractive force in the direction of the minumum. The spatial symmetry is here broken by the sawtooth-shape of the potential, while the time-reversal symmetry is broken by the Brownian motion of the particles.

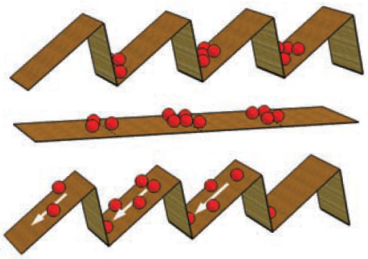

Figure 1.4: Classical ratchet using Brownian motion (Source: [27])

This effect is caused by the classical effect of dissipation which is absent in an ideal superfluid. Classical ratchets are subject to study due to several applications in the nanotechnology sector. For instance work has been published in the fields of protein engines [28], biology-inspired organic as well as inorganic nanodevices and, as described above, brownian motors [29], just to mention a few.

On the contrary part, little is known about the ratchet effect in the scope of quantum mechanics. This is partly due to the challenge in the experimental realization of suitable ratchet potentials. Nevertheless there are some efforts in realizing experiments concerning quantum ratchets [30] and also in the context of δ-kicked quantum ratchets [31] and. For example the rectification of quantum fluctuations using semiconductor hetero-structures has been observed [32].

In contrast to classical ratchet a quantum ratchet works devoid of dissipative processes. Directed motion of particles happens because of the breaking of spatiotemporal symmetries [27]. This is analogue to the sawtooth form of the potential in figure (1.4). Furthermore the time-inversion symmetry, which is in the classical example broken by the Brownian motion needs to be broken.

In this thesis we use the fact that with a periodically modulated Hamiltonian one can break the systems symmetries and therefore obtain a ratchet effect for a weakly interacting bosonic lattice gas. The aim is to study this effect, evaluating the system parameters to enhance the symmetry breaking and thus to maximize the atomic current. To have a better understanding we analyse the role of the interactions in Chapter 4, and characterizing the system properties without interactions in Chapter 3 as well.

To justify the chosen parameters we use the Floquet theory in Chapter 4 to understand the eigenfrequencies in a perturbative approach and draw conclusions to different set-ups for the amplitude of the driving and later the interaction strengths.

In Chapter 5 we expand our view on strong interactions and therefore leave the proximity area of the Gross-Pitaevskii theory. To show whether the system shows chaotic characteristics in this regime we apply the method of a Poincare map. Moreover we are interested in the fact, if there are stable regions separated from chaotic orbits in phase space for high non-linearites.

2 Numerical methods for the simulation

We study the time-dependent Gross-Pitaevskii equation describing the dynamics of a Bose-Einstein condensate (BEC) in a one-dimensional optical lattice. Due to the non-linearity of eq. (1.43) a numerical method is needed to solve the problem. As a technique of choice we use a Runge-Kutta method with accuracy of $\mathcal{O}(\tau^4)$ to find iteratively the solution of the non-linear differential equation.

2.1 Runge-Kutta-method (4^{th}-order)

To introduce the technique let us start with an initial value problem defined by

$$\frac{d}{dt}y = f(y,t) \qquad \text{with} \quad y(t_0) = y_0. \tag{2.1}$$

The variable t is discretized in steps of τ. A Taylor expansion of $y(t)$ at $t' = t + \tau$ leads to an approximated expression for $y_{t+\tau}$. From now on the index i marks the value of $y(t)$ at t and $i+1$ the value at $t + 1\tau$ and so forth, leading to the expansion up to the desired accuracy p,

$$y_{i+1} = y_i + \tau f(t_i, y_i) + \frac{1}{2}\tau^2 \left[\frac{d^2}{dt^2}y_i\right] + \ldots + \frac{1}{p!}\tau^p y_i^{(p)} + \mathcal{O}(\tau^{p+1}). \tag{2.2}$$

Reclaiming the equation (2.2) in every derivative one obtains the recursive Runge-Kutta formulas which are for an accuracy up to an order of 4 given by [33]

$$y_{i+1} = y_i + \frac{1}{6}\left[c_1 + 2c_2 + 2c_3 + c_4\right] \tag{2.3}$$

with the constants $c_1, \ldots, c_4$

$$\begin{aligned}
c_1 &= \tau f(t_i, y_i), \\
c_2 &= \tau f(t_i + \frac{1}{2}\tau, y_i + \frac{1}{2}c_1), \\
c_3 &= \tau f(t_i + \frac{1}{2}\tau, y_i + \frac{1}{2}c_2), \\
c_4 &= \tau f(t_i + \tau, y_i + c_3).
\end{aligned}$$

This calculation is implemented in a `C-program` with recursive value assignments for the constants $c_1, \ldots, c_4$. The use of Richardson extrapolation [34] allows to push the accuracy to arbitrary good values. But with every gained higher accuracy a higher amount of

constants needs to be calculated. As a compromise between runtime and accuracy we decided to use the 4^{th}-order

2.2 Simulation of an finite real-space-lattice

As a start we will apply the Numeric method on a finite lattice with free ($V = 0$) identical particles, which is characterized by well-defined, discrete lattice points. The well-localization is simulated by the use of an complex array `Psi[N]`. The calculations are executed for an lattice with $N = 40$ sites and periodic boundary conditions ($\psi_{N+1} = \psi_1$). The time discretization is chosen as $\tau = 0.01$. Further there were investigated two different initial conditions.

2.2.1 Gaussian initial condition

The first choice of initial conditions is a normalized gaussian distribution, without any momentum component:

$$\psi_j(t=0) = C \exp\left[-\frac{1}{2}\left(\frac{j-\mu}{\sigma}\right)^2\right] . \tag{2.4}$$

The center of the Gaussian μ is set in the middle of the lattice at $\frac{N}{2}$, and the standard deviation is selected to be $\sigma = \frac{N}{2}$. The Schrödinger equation for a free particle, with Gaussian initial distribution (2.4)

$$-\frac{\hbar^2}{2m}\partial_x^2 \psi = i\hbar\partial_t \psi , \tag{2.5}$$

must be solved. A ansatz for the wave function in equation (2.5) is given by the sum over every possible plane wave under the constraint that $\frac{\hbar^2 k^2}{2m} = \hbar\omega$,

$$\psi(\vec{r}, t) = \int \frac{d\vec{k}}{2\pi} \psi_{\vec{k}} \exp\left[i\left(\vec{k}\vec{r} - \frac{E_{\vec{k}}}{\hbar}t\right)\right] . \tag{2.6}$$

An explicit perform of a fourier-transformation and the back-transformation to real-space leads to the result, that the width of the Gaussian distribution σ_t increases with time, depending on the initial standard deviation $\sigma_{t=0}$.

The result of the Runge-Kutta method for the time-evolution in equation (1.50) of the wave function is plotted in figure (2.1). Due to the periodic boundary conditions the decay

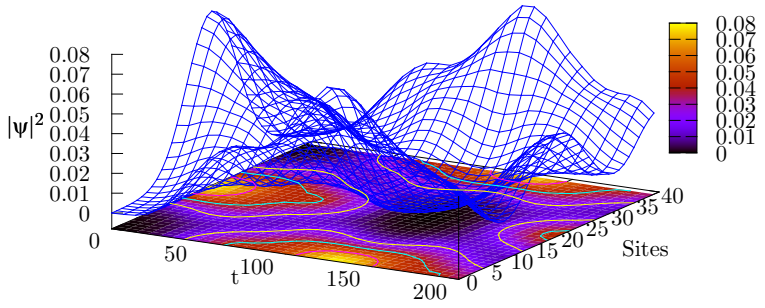

Figure 2.1: Time-evolution of $|\psi_k^2|$ with Gaussian initial conditions

evokes a periodic oscillation of the maximum in the plot between the center and the borders of the lattice because of the additive overlap of the circular floating wave function. Thus the theoretical model could be reproduced with a numeric calculation.

2.2.2 Well-localized initial condition

Another possibility to initialize the wave function is to constrict the probability density $|\psi|^2$ to one single site. So the initial condition is given by

$$\psi_j(t=0) = \delta(j-\chi). \tag{2.7}$$

where χ is the chosen site with $|\psi_\chi|^2 = 1$. We set χ in the middle of the lattice at $\frac{N}{2}$.

Analogue to section (2.2.1) the fourier-transform of equation (2.7) must be calculated, to get the time-dependence of ψ in real-space. The singularity is include by the fact that the energy dependence $E(k)$ is a cosine of k, so that $v_k = \frac{d\omega}{dk}$ is a sine-function. The back-transformation gives then a classical expectation, with the property of the δ-function $\delta(f(x)) = \frac{1}{|f'(x)|}$,

$$n(x,t) = \int_{-\pi}^{\pi} \delta(x - v_k t)\frac{dk}{2\pi} = \frac{1}{\left|\frac{\partial v_k}{\partial k}\right|}\bigg|_{v_k t = x} = \frac{1}{t\cos(k)}\bigg|_{\sin(k)=\frac{x}{t}} = \frac{1}{t\sqrt{1-\left(\frac{x}{t}\right)^2}} = \frac{1}{\sqrt{t^2-x^2}}\,. \tag{2.8}$$

The contour-plot in figure (2.2) shows the wave function behaviour. It is clearly visible,

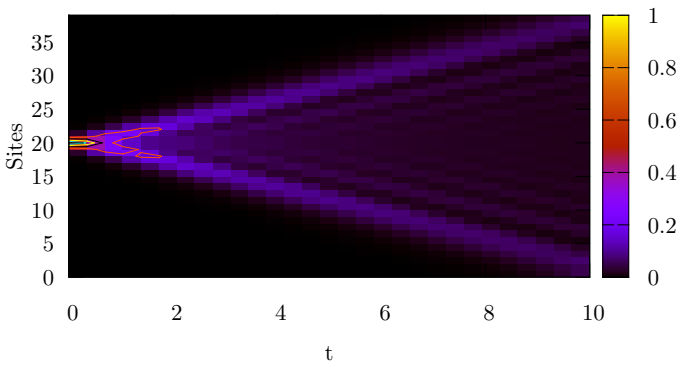

Figure 2.2: Contour-plot for $|\psi|^2$ with well-localized initial conditions

that the former δ-peak moves to the borders of the lattice. Again this matches with the analytic expectations. In conclusion one can say, that the Runge-Kutta method applied to the time-dependent mean field theory of the Hubbard model is quantitatively consistent with the analytic calculation. As a next step we concentrate on the realization of the ratchet in an infinite lattice system implementing the proper breaking of symmetries and investigate the resulting atomic current.

3 Non-interacting quantum ratchets

In this chapter we will present a non-interacting model, so that $g = 0$ in the discretized Gross-Pitaevskii equation (1.50). The first step for obtaining a ratchet effect is to break the spatial symmetry of the lattice in form of a alternating hopping-parameter J. More precisely every second barrier has the same value for J in the following named J_1 and J_2, which are from now on treated as time-dependent. This modulation is easy to realize in an optical lattice by modulating one laser with the doubled wavelength of the counter-propagating one. Thus one can divide the lattice into subdomains, each containing two lattice points, as sketched in figure (3.1). The two points in each box are denoted by L for left and R for right. In addition a local potential should be also used, to break spatial symmetry.

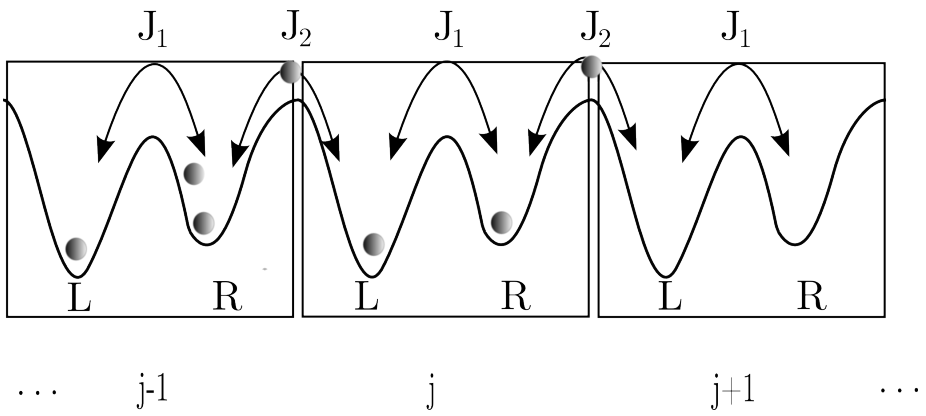

Figure 3.1: System with alternating hopping parameters J_1, J_2

The Hamiltonian for this problem featuring cells of two differing sites is then with the discrete form of the kinetic energy (1.46) and the potential (1.48) given by

$$\mathcal{H} = \sum_j \Big[- J_1(t) \left(\hat{\psi}^\dagger_{jL} \hat{\psi}_{jR} + \hat{\psi}^\dagger_{jR} \hat{\psi}_{jL} \right) - J_2(t) \left(\hat{\psi}^\dagger_{jR} \hat{\psi}_{j+1\,L} + \hat{\psi}^\dagger_{j+1,L} \hat{\psi}_{jR} \right) . \\ + V_{j,L}\, \hat{\psi}^\dagger_{j,L} \hat{\psi}_{j,L} + V_{j,R}\, \hat{\psi}^\dagger_{j,R} \hat{\psi}_{j,R} \Big] \tag{3.1}$$

Moreover we consider not longer a finite but an infinite lattice. As it will turn out later it is convenient to do a fourier transformation on the Hamiltonian and change into k-space, which will be the next operation.

3.1 Transformation to k-space

We start with the real-space Hamiltonian for a free particle, given by equation (3.1) with $V_{j,\sigma} = 0$, and the tight-binding approch. The discrete Fourier transformations of the form

$$\hat{\psi}_{j\sigma} \longrightarrow \sum_k \hat{\psi}_{k\sigma} e^{-ikj} \qquad \text{and} \qquad \hat{\psi}^\dagger_{j\sigma} \longrightarrow \sum_k \hat{\psi}^\dagger_{k\sigma} e^{ikj}, \tag{3.2}$$

is performed, with $\sigma \in \{L, R\}$. Using the discrete δ-function $\delta_{kk'} = \sum_j e^{-i(k-k')j}$, $\hat{\mathcal{H}}$ is calculated in the following way.

$$\begin{aligned}\hat{\mathcal{H}} = \sum_j \Bigg[& -J_1(t) \left(\sum_{k,k'} \hat{\psi}^\dagger_{k'L} e^{ik'j} \hat{\psi}_{kR} e^{-ikj} + \sum_{k,k'} \hat{\psi}^\dagger_{kR} e^{ikj} \hat{\psi}_{k'L} e^{-ik'j} \right) \\ & -J_2(t) \left(\sum_{k,k'} \hat{\psi}^\dagger_{k'R} e^{ik'j} \hat{\psi}_{kL} e^{-ik(j+1)} + \sum_{k,k'} \hat{\psi}^\dagger_{kL} e^{ik(j+1)} \hat{\psi}_{k'R} e^{-ik'j} \right) \Bigg]\end{aligned} \tag{3.3}$$

So the Hamiltonian becomes block-diagonal with the blocks

$$\mathcal{H}_k = \sum_k \hat{h}_k = \sum_k \Big\{ -J_1(t) \left[\hat{\psi}^\dagger_{kL} \hat{\psi}_{kR} + \hat{\psi}^\dagger_{kR} \hat{\psi}_{kL} \right] - J_2(t) \left[e^{-ik} \hat{\psi}^\dagger_{kR} \hat{\psi}_{kL} + e^{ik} \hat{\psi}^\dagger_{kL} \hat{\psi}_{kR} \right] \Big\}. \tag{3.4}$$

To justify later that a computed atomic current is detected due to a ratchet effect, we investigate the case without initial momentum ($k = 0$). The Hamiltonian of the system is in this constraint

$$\hat{\mathcal{H}}_{k=0} = -\Big(J_1(t) + J_2(t) \Big) \left[\hat{\psi}^\dagger_L \hat{\psi}_R + \hat{\psi}^\dagger_R \hat{\psi}_L \right]. \tag{3.5}$$

A convenient basis to represent the operators with matrices is the basis for the two sites L and R

$$\mathbb{B} = \{ L = (1,0)^T, R = (0,1)^T \}. \tag{3.6}$$

Using equation (1.26) and the field operators as funcitons of the ladder operators, the matrix-representation of any operator $\hat{\mathcal{O}}$ in the system of L and R is obtained by

$$\begin{aligned}\hat{\mathcal{O}} = \sum_{\alpha,\beta} \hat{\psi}^\dagger_\alpha \hat{\mathcal{O}} \hat{\psi}_\beta = {} & \hat{\psi}^\dagger_L \hat{\psi}_L \begin{pmatrix} 1 & 0 \end{pmatrix}^* \begin{pmatrix} a & b \\ c & d \end{pmatrix} \begin{pmatrix} 1 \\ 0 \end{pmatrix} + \hat{\psi}^\dagger_L \hat{\psi}_R \begin{pmatrix} 1 & 0 \end{pmatrix}^* \begin{pmatrix} a & b \\ c & d \end{pmatrix} \begin{pmatrix} 0 \\ 1 \end{pmatrix} \\ & + \quad \hat{\psi}^\dagger_R \hat{\psi}_L \begin{pmatrix} 0 & 1 \end{pmatrix}^* \begin{pmatrix} a & b \\ c & d \end{pmatrix} \begin{pmatrix} 1 \\ 0 \end{pmatrix} + \hat{\psi}^\dagger_R \hat{\psi}_R \begin{pmatrix} 0 & 1 \end{pmatrix}^* \begin{pmatrix} a & b \\ c & d \end{pmatrix} \begin{pmatrix} 0 \\ 1 \end{pmatrix} \\ = {} & a \hat{\psi}^\dagger_L \hat{\psi}_L + b \hat{\psi}^\dagger_L \hat{\psi}_R + c \hat{\psi}^\dagger_R \hat{\psi}_L + d \hat{\psi}^\dagger_R \hat{\psi}_R.\end{aligned} \tag{3.7}$$

In this form the Hamiltonian (3.5) can be written as

$$\hat{\mathcal{H}}_{k=0} = -\Big(J_1(t) + J_2(t)\Big). \begin{pmatrix} 0 & 1 \\ 1 & 0 \end{pmatrix} \tag{3.8}$$

Numerically $\hat{\psi}_\sigma$ and $\hat{\psi}_\sigma^\dagger$ are then, with the mean-field approach, treated as complex functions and are associated with the arrays `Psi[i]` and `Psi*[i]`, where `i` marks the site of the lattice in k-space (L or R). Another way to write the Hamiltonian is to separate the time-dependent from the constant part. In this sense we can rewrite equation (3.5) as

$$\hat{\mathcal{H}} = \hat{\mathcal{H}}_0 + \delta\mathcal{H}_t. \tag{3.9}$$

3.2 System with absent potential

The analytic solution for a system with the Hamiltonian in equation (3.5) can be calculated comparatively simple. So it can serve as a testing ground for the numerical methods, which are applied later to the non-linear Gross-Pitaevskii equation. In this chapter we will first consider the case of absent potential and later implement several kinds of periodic potentials.

At first the analytic solution for equation (3.5) is sketched, to maintain the average density $\langle n_\sigma \rangle_t$ of the two sites *Left* and *Right*. First of all the Hamiltonian is diagonalized by performing the following basis transformation on the operators $\hat{\psi}_L$ and $\hat{\psi}_R$

$$\hat{\psi}_+ = \frac{1}{\sqrt{2}}\left(\hat{\psi}_R + \hat{\psi}_L\right), \qquad \text{and} \qquad \hat{\psi}_- = \frac{1}{\sqrt{2}}\left(\hat{\psi}_R - \hat{\psi}_L\right). \tag{3.10}$$

The diagonalized form of the Hamiltonian is then with $J(t) = J_1(t) + J_2(t)$ and $\hat{n}_\pm = \hat{\psi}_\pm^\dagger \hat{\psi}_\pm$

$$\hat{\mathcal{H}} = -J(t)\left(\hat{n}_+ - \hat{n}_-\right). \tag{3.11}$$

The Heisenberg-equation together with the use of the commutation relations of equation (1.20), gives the time-evolution for the operators $\hat{\psi}_\pm$.

$$i\partial_t \hat{\psi}_\pm = -J(t)(\pm 1)\hat{\psi}_\pm \tag{3.12}$$

With equation (3.12) and using integrable functions for $J(t)$ it is possible to calculate first $\hat{\psi}_{\pm}(t)$ and then then operate the reverse transformation of equation (3.10) to get $\hat{\psi}_{\sigma}(t)$ and finally the average density per site $\langle n_{\sigma}\rangle(t)$ with $\langle n_{\sigma}\rangle(t) = \hat{\psi}^{\dagger}_{\sigma}(t)\psi_{\sigma}(t)$.

A general case for periodic time-dependent hopping is given by

$$J_i(t) = J_0, i + \delta_i \cos(\omega t). \tag{3.13}$$

With this strategy for the analytic solutions of equation (3.12) for the two cases for the kinetic energy

$$J_i(t) = J_{0,i} \qquad i \in \{1, 2\}, \tag{3.14}$$

$$J_i(t) = J_0, i + \delta_i \cos(\omega t), \tag{3.15}$$

are then given by

$$\hat{b}_{\pm}(t) = \exp\Big[\pm i(J_{0,1} + J_{0,2})t\Big] \qquad \text{for } \delta_i = 0 \tag{3.16}$$

$$\text{and} \qquad \hat{b}_{\pm}(t) = \exp\Big[\pm i\left((J_{0,1} + J_{0,2})t + \frac{\delta_1 + \delta_2}{\omega}\sin(\omega t)\right)\Big] \qquad \text{for } \delta_i \neq 0 \tag{3.17}$$

After carrying out the back transformation of equation (3.10) it is possible to extract the theoretic expectations for the densities for the sites L and R. It turns out that these are linear combinations of $\cos^2$- and $\sin^2$-functions, weighted by the initial distribution of the two sites represented by $\hat{n}_L(t = 0)$ and $\hat{n}_R(t = 0)$. In the following example we have chosen for simplicity the initial conditions as $|L, R\rangle = |0, 1\rangle$. The analytic functions for the mean-densities in this special case are

$$\langle n_R\rangle(t) = \langle b^{\dagger}_R(t) b_R(t)\rangle = \cos^2\left(J_0 t + \frac{\delta}{\omega}\sin(\omega t)\right), \tag{3.18}$$

$$\langle n_L\rangle(t) = \langle b^{\dagger}_L(t) b_L(t)\rangle = \sin^2\left(J_0 t + \frac{\delta}{\omega}\sin(\omega t)\right). \tag{3.19}$$

where $J_0 = J_{0,1} + J_{0,2}$ and $\delta = \delta_1 + \delta_2$. So a striking property of the system is, that it has an intrinsic period given by J_0, which occurs even if there is now external time-periodic modulation, so when $\delta_i = 0$.

These solutions are now reproduced by numerical calculations using the introduced Runge-Kutta method. The results for constant hopping parameters are displayed for the site R in

figure (3.2). Panel (3.2) (a) shows the squared cosine shape of the curve, with the intrinsic frequency J_0 as it was predicted in equation (3.18).

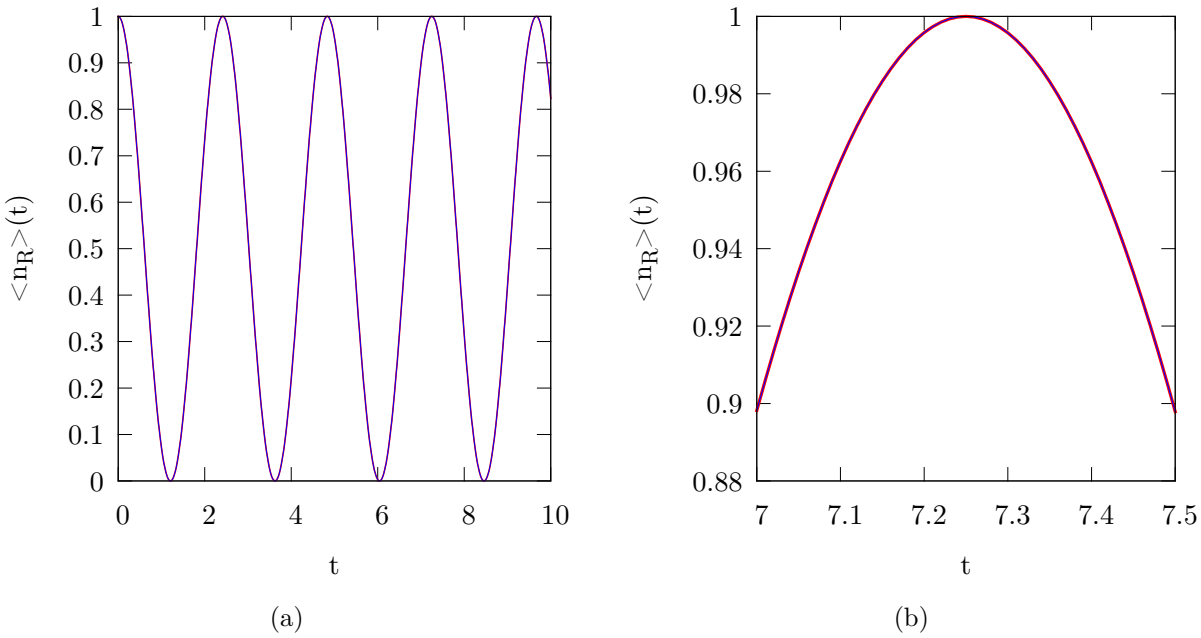

Figure 3.2: Time-evolution of $\langle n_R \rangle(t)$ with $J_i = const.$, where the red line is the numerical data and the blue line the theoretical results.
Panel (a) shows the long-term evolution while panel (b) presents an insight of (a) to emphasize the agreement of numerics with theory. The chosen hopping-parameters are $J_{0,1} = 1.0$, $J_{0,2} = 0.3$.

Panel (3.2)(b) illustrates the very good agreement of the Runge-Kutta values with respect to the theoretic expectations.

In the next step, the time-dependence of the J_i is added. For this purpose a cosine-term with a frequency ω is added like it was discussed in equation (3.15). In order to see a deviation from the squared cosine the amplitudes of the time dependent part must be setted to be of the same order as J_1 and J_2, they are chosen as $\delta_1 = 1.00$ and $\delta_2 = 0.21$. Again the numerical data is plotted in figure (3.3) against the analytic results. Figure (3.3)(b) shows the numeric reproduction reproduction of the theory.

Further the periodicity in figure (3.3)(a) becomes more complex. Nevertheless there can still be identified a period if ω is commensurate with J_0. This is shown in figure (3.4), which is the same calculation as before in a wider range. The periodic shift arises here in form of a square sine-function. Here no temporal or spatial symmetries were broken, thus

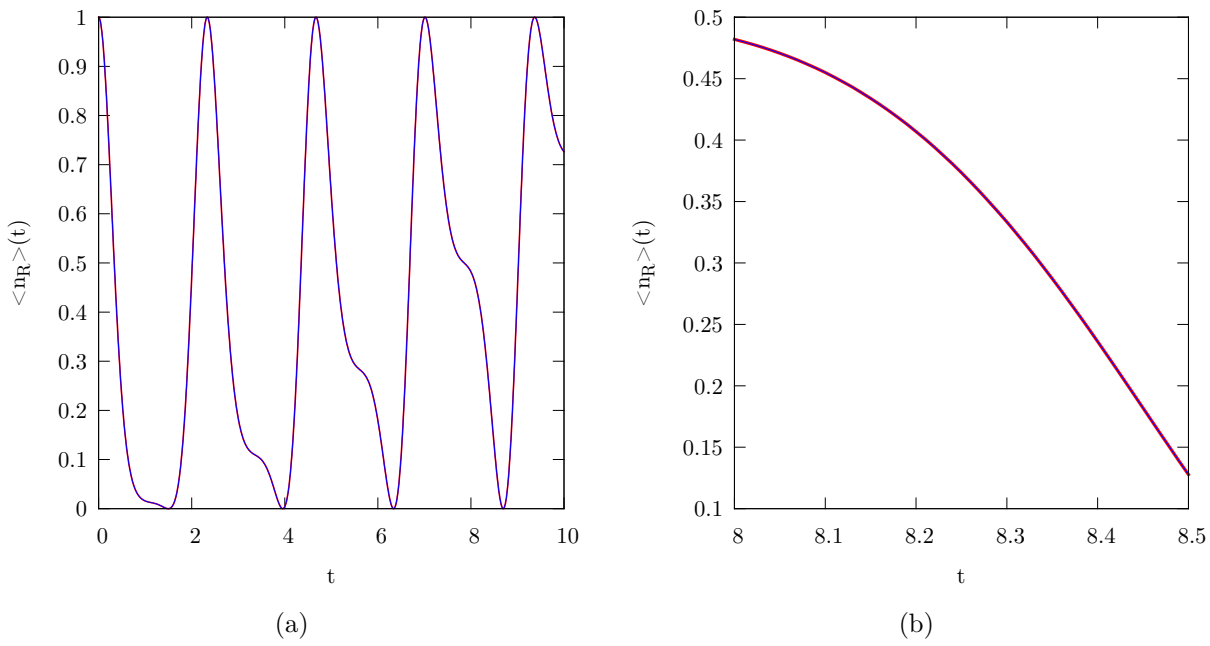

Figure 3.3: Time-evolution of $\langle n_R \rangle(t)$ for $J_i = J_i(t)$ with the parameters: $J_{0,1} = 1.0$, $J_{0,2} = 0.3$, $\delta_1 = 1.0$, $\delta_2 = 0.21$, $\omega = 2.8$, again red stands for numerical data and blue for theoretical calculations
(a) shows the curve's shape and (b) a zoom in a small interval of (a)

there should be no ratchet effect and consequently no atomic current in this system. In order to analyse this fact, the current using second quantisation is introduced.

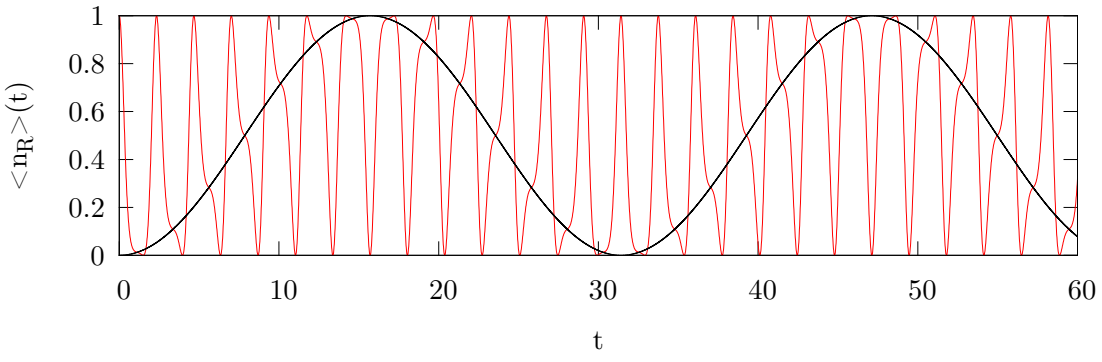

Figure 3.4: Complex periodicity of the density $\langle n_R \rangle(t)$. The black line emphasizes the periodicity which has the form of $\sin^2(ct)$

3.2.1 Current-operator

The current $\hat{j}$ is defined by the number of particles, which move from one site to another one. Because of the thight-binding regime, this process is limited to the neighbour sites. In the language of second quantisation the motion of particles is described as the destruction in one site and the creation in the adjacent one. The probability of such an event is determined by the hopping-parameters.

The current operator is specified by the continuity equation

$$\partial_t \left(\hat{\psi}_i^\dagger \hat{\psi}_i\right) = j(\text{ hopping from } i+1 \text{ to } i\ ) - j(\text{ hopping from } i \text{ to } i+1\ ) \tag{3.20}$$

and therefore is given by $-J\hat{\psi}_i^\dagger \hat{\psi}_{i+1}$ subtracted by $-J\hat{\psi}_{i+1}^\dagger \hat{\psi}_i$. But since $\hat{j}$ is an observable, it must be hermitian, thus $\hat{j}^\dagger = \hat{j}$. To guarantee this property, one of the summands is multiplied with i and the other one with $-i$. So the final operator for the atomic current has the following form

$$\hat{j} = -J\, i\, \left(\hat{\psi}_{i+1}^\dagger \hat{\psi}_i - \hat{\psi}_i^\dagger \hat{\psi}_{i+1}\right). \tag{3.21}$$

Physically the total net-current is computed here by subtracting the current in one direction from the one in its counter-direction.

If we return to figure (3.1), the process for site (j, L) is for the hopping in the left direction $-J_2\hat{\psi}_{j-1,R}^\dagger \hat{\psi}_{j,L}$ and in the right direction $-J_1\hat{\psi}_{j,R}^\dagger \hat{\psi}_{j,L}$. The same procedure is operated for site (j, R), so that the total current for all cells is divided into a current inside the cell and one flowing out of it. The current for the whole lattice is then given by the sum over all sites j

$$\hat{j} = \sum_j \left[(-J_1(t))i\left(\hat{\psi}_{jL}^\dagger \hat{\psi}_{jR} - \hat{\psi}_{jR}^\dagger \hat{\psi}_{jL}\right) + (-J_2(t))i\left(\hat{\psi}_{jR}^\dagger \hat{\psi}_{j+1,L} - \hat{\psi}_{j+1,L}^\dagger \hat{\psi}_{jR}\right)\right]. \tag{3.22}$$

Now, analogue to section (3.1) a Fourier-transformation is performed and the restriction to $k = 0$ leads to the following form of the operator

$$\hat{j} = -(J_1(t) - J_2(t))i\left(\hat{\psi}_L^\dagger \hat{\psi}_R - \hat{\psi}_R^\dagger \hat{\psi}_L\right). \tag{3.23}$$

In the simulation, the operator is a matrix acting on the vector `Psi[]`. The expectation value is then calculated with the standard rules of quantum mechanics and the use of

equation (3.7) for the matrix-representation of the second-quantisation operator,

$$\begin{aligned}\langle\hat{j}\rangle &= \langle\psi|\hat{j}|\psi\rangle = -(J_1(t) - J_2(t))\, i\, \langle\psi|\hat{\psi}_L^\dagger\hat{\psi}_R - \hat{\psi}_R^\dagger\hat{\psi}_L|\psi\rangle \\ &= (J_1(t) - J_2(t)) \begin{pmatrix}\psi_L^* \\ \psi_R^*\end{pmatrix} \underbrace{\begin{pmatrix}0 & -i \\ i & 0\end{pmatrix}}_{=\sigma_y} \begin{pmatrix}\psi_L \\ \psi_R\end{pmatrix} . \end{aligned} \tag{3.24}$$

So one can say, that the Pauli matrix σ_y can be identified with the atomic current. From this follows the numerical formula for the current, which can be written as

$$\texttt{j =-i(J1-J2)(Psi[L]*Psi[R] - Psi[R]*Psi[L])}. \tag{3.25}$$

For the non-potential case, it is possible to specify the time-dependence of $\hat{j}$ knowing $\hat{\psi}_\sigma$

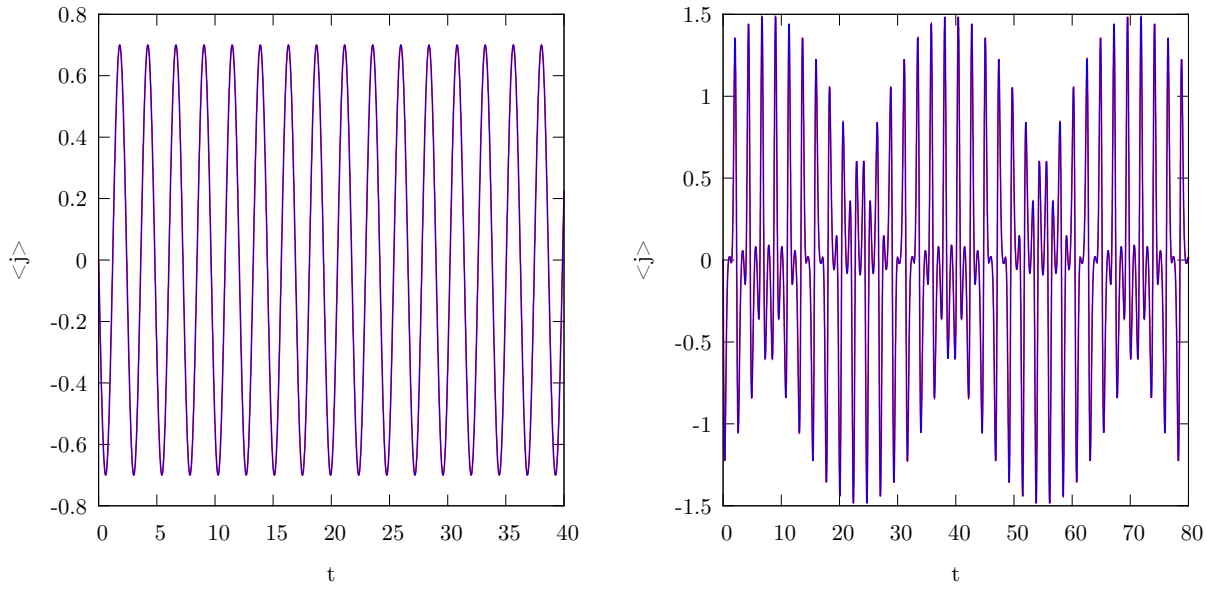

(a) (b)

Figure 3.5: Time-evolution of the current for a constant (left) and a time dependent (right) hopping. Same parameters as before

and $\psi_\sigma^\dagger$, from the solution of the Heisenberg equation of the fourier-transformed diagonalized Hamiltonian $\mathcal{H}_k$. This has been done for the two considered cases. The formula for

the current turns out to be for the initial condition $|L, R\rangle = |0, 1\rangle$

$$\langle j(t)\rangle = -(J_1(t) - J_2(t)) \sin\left[2\left\{(J_{0,1} + J_{0,2})\, t + \frac{\delta_1 + \delta_2}{\omega} \sin(\omega t)\right\}\right]. \tag{3.26}$$

Figure (3.5) displays both, the theoretical and numerical results for the two hopping-instances, which match in a very good accuracy. But in both cases, the current oscillates around zero. The consequence of this is that there does not exist a net-current over a long time interval. In conclusion there is no ratchet effect in this system, as it was suggested in the interpretation of the figures (3.2) and (3.4).

3.2.1.1 Mean current

The tendency of the current should be analysed more accurately. To gain the mean-value of the current, the current is integrated over time. This value then converges after a long time to a fix value. In the above considered system this limit is zero, due to periodicity of the current. The integrated current is computed continuously for every time t as

$$\langle j\rangle(t) \equiv j_{int}(t) = \frac{1}{t}\int_0^t j(t')dt'. \tag{3.27}$$

To approximate the limit $\lim_{t\to\infty}\langle j\rangle(t)$ the integrated current is averaged over an time interval Δt at the end of the whole calculated interval $[0, t_f]$. In the numerics the current is calculated for discrete times with the discretization time τ, over an interval where one can consider the system to be stabilized

$$\lim_{t\to\infty}\langle j\rangle(t) \cong j_{mean}(t_f, \Delta t) \equiv \frac{1}{\Delta t}\sum_i^N j_{int}(t_i), \tag{3.28}$$
$$\text{with} \quad N = \frac{\Delta t}{\tau} \qquad \text{and} \quad t_i = t_f - (N - i)\tau.$$

This is the quantity we will refer to later as the integrated current, or more roughly just as the current. It is important to pick this interval Δt not to short, to compensate small oscillations of the current, and not to long, for not entering the highly oscillating zone in the small time-values and remain in a section with small variation.

As expected figure (3.6) illustrates that the mean-current vanishes for the case of $\delta_i \neq 0$ considered above.

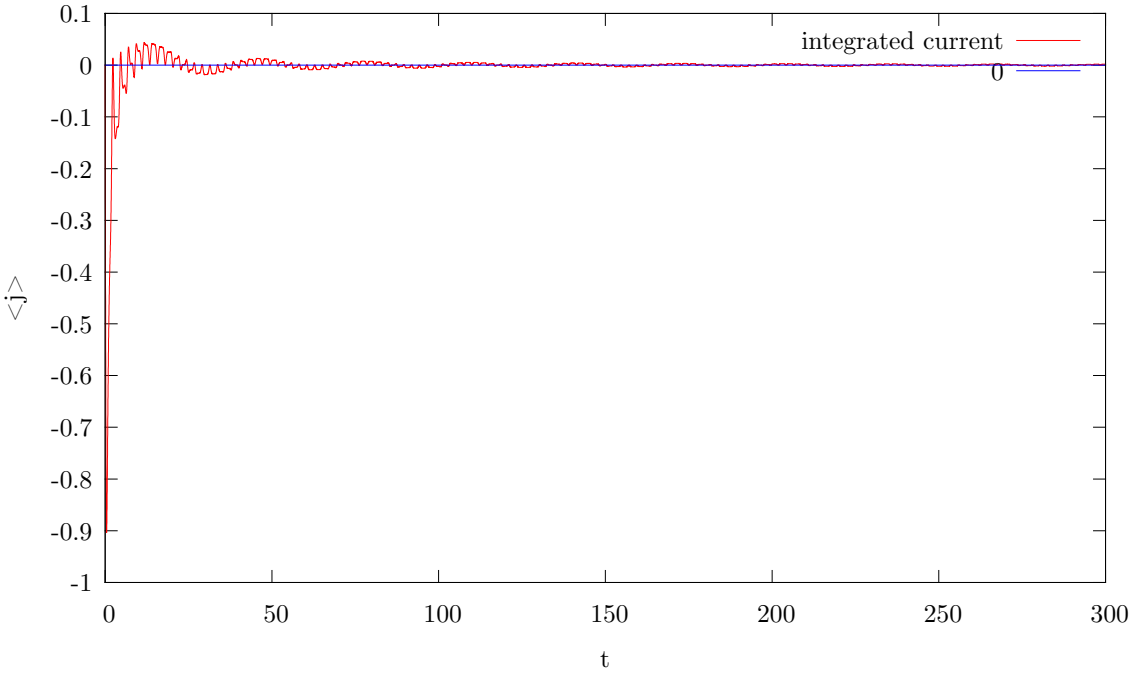

Figure 3.6: Asymptotic behaviour of the integrated current as a function of time. The blue line guides the eye.

3.3 System in the presence of a potential

In section (3.2) we have seen that there is no net-current in a system with absent potential, even if the hopping parameters have different values and oscillate time. As a next approach we will add a potential with a site-alternating positive and and negative sign

$$V(t) = \begin{cases} V(t) & \text{for L,} \\ -V(t) & \text{for R.} \end{cases} \tag{3.29}$$

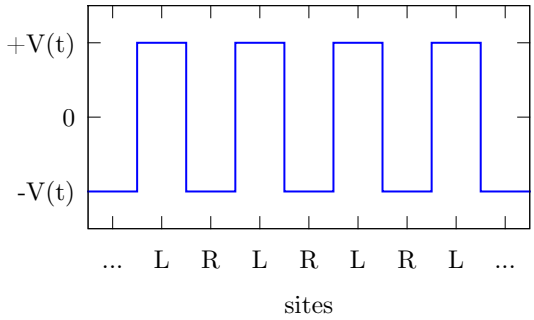

The potential-operator acts on the particles in each site so that it can be identified with the number operator $\hat{b}_\sigma^\dagger \hat{b}_\sigma$. In the manner of equation(3.7) the Hamiltonian has then the form

$$\mathcal{H} = \begin{pmatrix} V(t) & -(J_1(t) + J_2(t)) \\ -(J_1(t) + J_2(t)) & -V(t) \end{pmatrix} . \tag{3.30}$$

The form of the potential helps to break the spatial symmetry. But there still exist symmetry-axes namely a mirror on a lattice sites which is not broken via the potential but using the different hopping to the left and right. Further we will investigate the characteristics of the system for a broken time-reversal symmetry (3.32), and compare it to one with a constant potential

$$V(t) = V_0 = const., \tag{3.31}$$

$$V(t) = V_0 + \delta_V \cos(\omega t + \varphi). \tag{3.32}$$

Here φ is an added phase in the potential and therefore breaks the time-reversal symmetry in combination with the cosine-function of the hopping-parameters in equation (3.15).

In figure (3.7) the six possible combination of constant and time-dependent J with absent, alternating constant and alternating time-dependent potential are plotted for the last 200 time-units to point out the long-term behaviour of the current. The options are assigned to the plots via the table below. The average-value of the current in this region is treated as the final current of the ratchet system since its remaining oscillations are insignificant. The plots show, that there is only a finite integrated current, if the potential as well as the hopping-parameters are time-dependent. In all other options, the integrated current oscillates around zero (fig. 3.7 d,e) or approaches zero from one direction (fig. 3.7 a,b,c).

Figure	J	V
(a)	$J = const.$	$V = 0$
(b)	$J = const.$	$V = \pm V_0$
(c)	$J = const.$	$V = \pm V(t)$
(d)	$J = J(t)$	$V = 0$
(e)	$J = J(t)$	$V = \pm V_0$
(f)	$J = J(t)$	$V = \pm V(t)$

As a first qualitative result it is appropriate to say, that there remains a finite unidirectional current only if the time-reversal symmetry is broken. This is demonstrated more detailed later in the discussion of the phase-shift φ in section(4.1). In general all parameters were up to now arbitrary chosen. It is now the task to examine the behaviour of the system, in the sense of maximazing the current by changing the parameters in a systematic way.

An additional discovered effect is, that the net-current vanishes if the relation between the constant hopping parameters to the amplitudes of the corresponding time-dependencies is

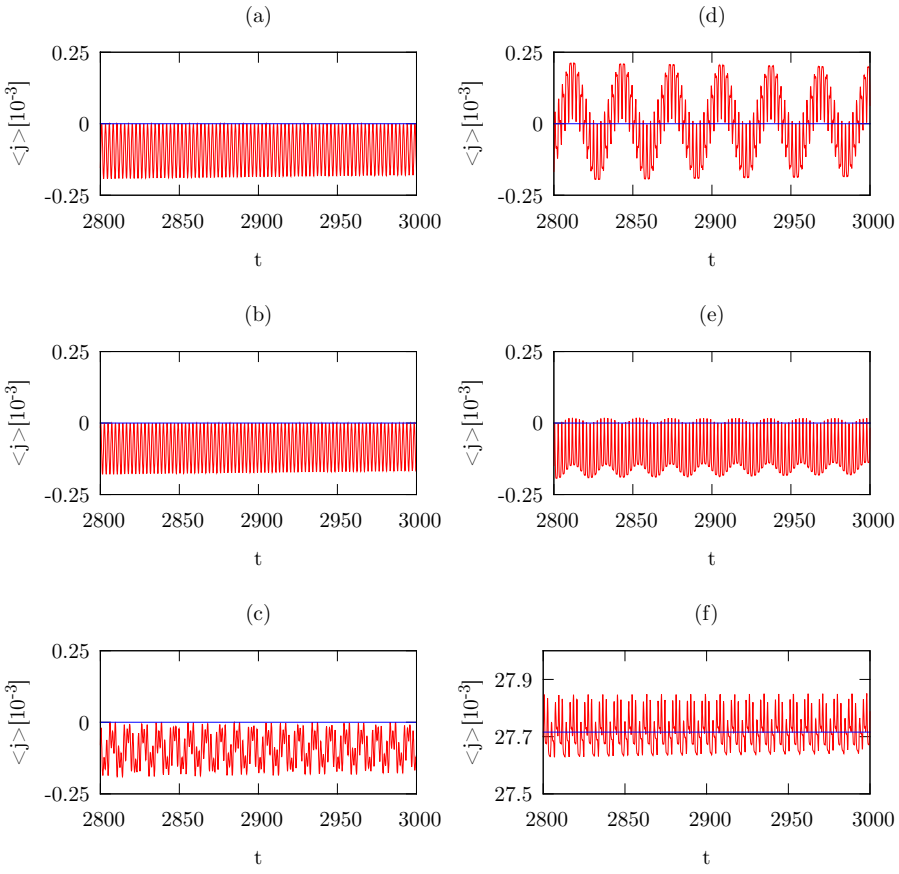

Figure 3.7: Long-time development of the integrated current for the set-ups: Parameters: $J_{01} = 1.0$, $J_{02} = 0.3$, $\delta_1 = 1.0$, $\delta_2 = 0.21$, $V = 0.7$, $\delta_V = 0.7$, $\omega = 2.8$, $\varphi = \frac{\pi}{2}$, for a assignment to the plottet data revisit the table on page 33

chosen to be equal like

$$J_1(t) = J_{0,1}(1 + \delta\cos(\omega t)), \tag{3.33}$$

$$J_2(t) = J_{0,2}(1 + \delta\cos(\omega t)). \tag{3.34}$$

To avoid this we introduce a further parameter δ_{rel} for second hopping parameters, so that the amplitude of its time dependence is given by $\delta_2 = \delta \cdot \delta_{rel}$. The pontential's factor δ_V is implemented as as $\delta_V = \delta \cdot V_0$.

4 Quantum ratchets considering weak interactions

In the set-up of an optical lattice it is possible to regulate the interaction-strength, so that, in contrast to solids, several different options can be realized experimentally. The problem discussed in this chapter contains only weak-interactions for a g of the order of a tenth of the kinetic or potential energy. For the weakly interacting case we employ the Gross-Pitaevskii equation (1.43). The behaviour for greater interactions, that is to say with greater coefficients g is outlined later in Chapter 5.

4.1 Role of the time-reversal symmetry in the ratchet

In the following it is studied to what extend the current is influenced by the interactions in comparison to the non-interacting system of Chapter 3. Furthermore the influence of the time-reversal symmetry breaking caused by φ in equation (3.32) is investigated. For this purpose the asymptotic current is plotted for several values of the interaction strength g.

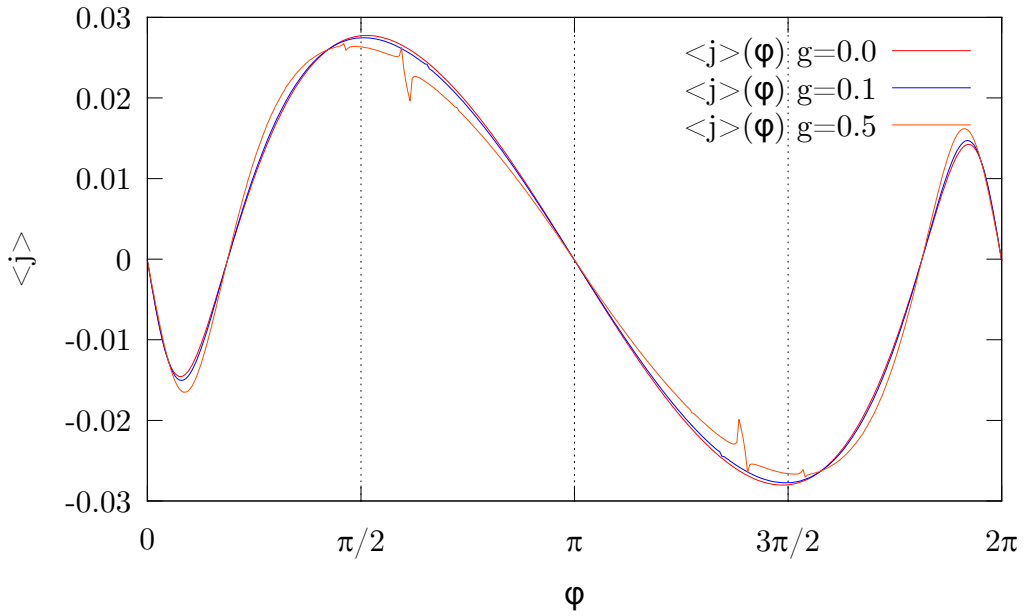

Figure 4.1: $\langle j \rangle$ as a function of the phase shift φ for the interaction strength $g = 0.0, 0.1, 0.5$, the other parameters were chosen as above.

The results are shown in figure (4.1). It is clearly recognizable, that the current vanishes at the value of $\varphi = 0$ and $\varphi = \pi$. This matches the expectations since the absolute value of the cosine for the time-dependent potential has a periodicity of π. Consequently, the time-reversal symmetry between the potential V and the kinetic energy-terms J_1 and J_2 is

restored at points where φ is a integer multiple of π. This shows again, that there is only a non-vanishing asymptotic current, if the temporal symmetry is broken.

Another feature of the plot (4.1) is revealed by the fact, that the current is maximal around $\varphi = \frac{\pi}{2}(2n+1)$,where $n \in \mathbb{N}_0$. This originates in the property of the trigonometric functions that

$$\cos(x + (2n+1)\frac{\pi}{2}) = (-1)^{2n+1}\sin(x). \tag{4.1}$$

Since $\sin(x)$ and $\cos(x)$ are orthogonal with respect to the scalar product

$$\langle f, g\rangle = \frac{1}{\pi}\int_0^{2\pi} f(x)g(x)dx, \tag{4.2}$$

the temporal symmetry is maximally broken for $\varphi = (2n+1)\frac{\pi}{2}$. That is the reason why φ is chosen in most of the calculations in this thesis as $\frac{\pi}{2}$.

Remarkable is, that in the weakly-interacting regime the influence of the interactions are negligible. The curves of $g = 0$ and $g = 0.1$ coincide with a few small exceptions. With an increasing interaction term this agreement disappears as seen in the curve for $g = 0.5$. Moreover there occur small peaks, which are not discussed in more detailed in this thesis. But it is possible that they are caused by the fact that the interactions shifts the current-dependence of the driving and the peaks therefore stand in context to the resonance frequencies treated in section 4.2. In general one can say, that the behaviour of the weak-interacting system is comparable to the non-interacting system. This result coincides with the conclusions obtained in reference [5] but contrast sharply with [6], where a non-zero momentum is obtained with the help of interactions. It seems that in a stronger interacing environment the interaction strength influences the current, but since the Gross-Pitaevskii theory is constricted to weak interactions, we can not give any quantitative statement in this direction.

4.2 Quantum ratchet with variable driving-frequency

We investigate now the behaviour of the current while we change the driving-frequency ω of the system continuously. Before we analyse the numerical results, we examine the eigenfrequencies with the use of the Floquet theory. Thus the Ratchet Floquet-Hamiltonian $\mathcal{H}_F$ of equation (1.6) is needed. The matrix elements $(\hat{\mathcal{H}}_F)_{nm}$ are calculated using the

Floquet states of equation (1.7) given by

$$(\hat{\mathcal{H}}_F)_{nm} = \langle\phi_n(t)|\hat{\mathcal{H}}_F|\phi_m(t)\rangle = \int e^{i\mu_n t}\hat{\mathcal{H}}_F e^{-i\mu_m t}dt = \int e^{in\omega t}\left(\hat{\mathcal{H}} - i\partial_t\right)e^{-im\omega t}dt$$
$$= \int e^{in\omega t}\hat{\mathcal{H}}e^{-im\omega t}dt - i\int e^{in\omega t}\partial_t e^{-im\omega t}dt, \tag{4.3}$$

where the Floquet exponents $\mu_n = n\omega$ are identified with the driving frequency ω

$$(\hat{\mathcal{H}}_F)_{nm} = \int e^{i\omega nt}\hat{\mathcal{H}}e^{-i\omega mt} - \omega m\underbrace{\int e^{i\omega t(n-m)}dt}_{=\delta_{nm}}. \tag{4.4}$$

The Hamiltonian in second quantisation including potential and interaction is given by

$$\hat{\mathcal{H}} = (V(t) + g\,|\psi|^2)\hat{\psi}_L^\dagger\hat{\psi}_L - J(t)\hat{\psi}_L^\dagger\hat{\psi}_R - J(t)\hat{\psi}_R^\dagger\hat{\psi}_L + (-V(t) + g\,|\psi|^2)\hat{\psi}_R^\dagger\hat{\psi}_R, \tag{4.5}$$

what is equivalent to the matrix representation

$$\hat{\mathcal{H}} = \begin{pmatrix} V(t) + g\,|\psi|^2 & -J(t) \\ -J(t) & -V(t) + g\,|\psi|^2 \end{pmatrix}$$
$$= \underbrace{\begin{pmatrix} V_0 + g\,|\psi|^2 & -J_0 \\ -J_0 & -V_0 + g\,|\psi|^2 \end{pmatrix}}_{=\hat{\mathcal{H}}_0} + \underbrace{\begin{pmatrix} \delta_V\cos(\omega t + \varphi) & -\delta_J\cos(\omega t) \\ -\delta_J\cos(\omega t) & -\delta_V\cos(\omega t + \varphi) \end{pmatrix}}_{=\hat{\mathcal{H}}_t}. \tag{4.6}$$

In the following procedure we evaluate the matrix element of equation (4.4) for $\cos(\omega t + \varphi)$

$$\int e^{i\omega nt}\cos(\omega t + \varphi)e^{-i\omega mt}dt = \int e^{i\omega nt}\frac{1}{2}\left(e^{-i(\varphi+\omega t)} + e^{i(\varphi+\omega t)}\right)e^{-i\omega mt}dt$$
$$= \frac{1}{2}\int e^{-i\varphi}e^{i\omega t(n-(m+1))} + e^{i\varphi}e^{i\omega t(n-(m-1))}dt = \frac{1}{2}\left[e^{-i\varphi}\delta_{n,m+1} + e^{i\varphi}\delta_{n,m-1}\right], \tag{4.7}$$

and $\mathcal{H}_0$ which is time-independent and therefore diagonal

$$\int e^{i\omega nt}\hat{\mathcal{H}}_0 e^{-i\omega mt}dt = \hat{\mathcal{H}}_0\delta_{n,m}. \tag{4.8}$$

Concerning (4.7) and (4.8) the Floquet-Hamiltonian for the system is

$$\hat{\mathcal{H}}_F = \hat{\mathcal{H}}_0\delta_{n,m} + \frac{\delta_J}{2}\left[\delta_{n,m+1} + \delta_{n,m-1}\right]\sigma_x + \frac{\delta_V}{2}\left[e^{-i\varphi}\delta_{n,m+1} + e^{i\varphi}\delta_{n,m-1}\right]\sigma_z, \tag{4.9}$$

where n and m run from $-\infty$ to ∞ and represent matrix-blocks of the dimension 2×2. We now calculate the eigenfrequencies ω_0 for the non-interacting system without any time-dependence. So we just take $\hat{\mathcal{H}}_0$ into account. The Floquet matrix is then already block diagonal with the blocks $\hat{\mathcal{H}}_0$. To diagonalize the matrix completely, we only need to transform $\hat{\mathcal{H}}_0$, which results in a 2×2 matrix, with $\pm\omega_0 = \pm\sqrt{V_0^2 + J_0^2}$ on the diagonal. So the eigenvalues of the Floquet Hamiltonian are

$$n\omega \pm \omega_0. \tag{4.10}$$

If the time-dependent term $\hat{\mathcal{H}}_t$ in equation (3.9) is small compared to $\mathcal{H}_0$ a treatment within the framework of perturbation theory is justified. The energy in non-degenerated perturbation theory, up to second order of $\mathcal{H}_t$ is given by [35]

$$E_n \approx \epsilon_n + \langle n|\mathcal{H}_{F,t}|n\rangle + \sum_{m\neq n} \frac{|\langle m|\mathcal{H}_{F,t}|n\rangle|^2}{\epsilon_m - \epsilon_n} + \mathcal{O}(\mathcal{H}_{F,t}^2), \tag{4.11}$$

where ϵ_n and ϵ_m are the eigen-energies of the non-perturbative Floquet Hamiltonian $\hat{\mathcal{H}}_{F,0}$ calculated in (4.10). The second-order term reveals a singularity if the eigen-energies are degenerated $\epsilon_n = \epsilon_m$. So we expect resonance frequencies, where

$$n\omega + \omega_0 = m\omega - \omega_0 \Longrightarrow 2\omega_0 = \underbrace{(m-n)}_{=1}\omega. \tag{4.12}$$

Here $m - n = 1$ because the constant blocks $\mathcal{H}_0^n$ on the main-diagonal of the Floquet-Hamiltonian (4.9) can affect only the blocks $\mathcal{H}_0^{n-1}$ or $\mathcal{H}_0^{n+1}$ over the off-diagonal blocks of δ_J and δ_V. In higher order of perturbation theory we expect also resonances for $m - n = 2, 3, 4, \ldots$ as can be seen in figure 4.2.

Figure (4.2) shows the asymptotic current plotted for a continuously changing of the driving frequency. In contrast to the investigations before, here we used small amplitudes for $\mathcal{H}_t$ compared to those of $\mathcal{H}_0$. One can say, that in this regime the weakly interacting results coincides with the expectations from perturbation theory, as long as there are peaks at the harmonic frequencies of $2\omega_0$.

In the ratchet context the regime where $\mathcal{H}_t \ll \mathcal{H}_0$ is not considered in our previous set-up because we need to chose $\mathcal{H}_t \approx \mathcal{H}_0$, which means to have the amplitude of the time-dependence, of the same order as the constant time-independent amplitudes $J_{0,1}$, $J_{0,2}$ and

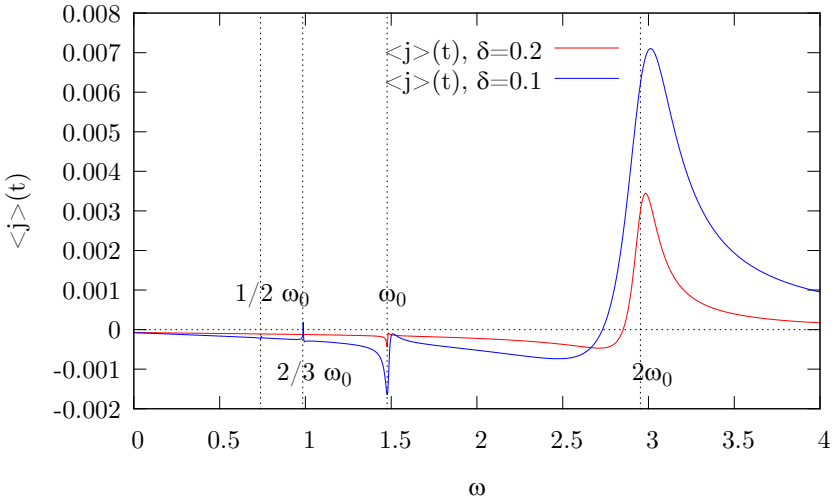

Figure 4.2: The asymptotic current is plotted versus the driving frequency for two values of $\delta\mathcal{H}_{F,t}$ with $\delta = 0.1$ and $\delta = 0.2$.

V_0. Figure (4.3) shows now a plot under these conditions. Instead of a sharp peak for

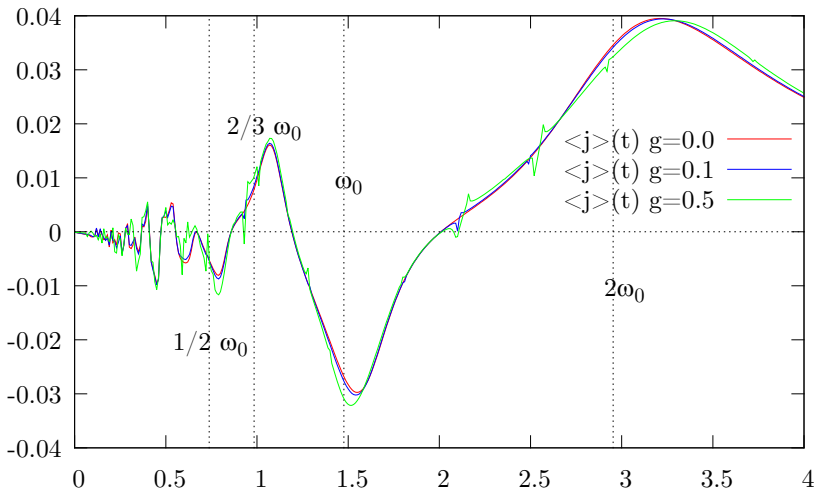

Figure 4.3: Driving frequency versus current with the time-dependent-term being of the same order as the constant amplitude ($\delta = 1$)

the harmonics of $2\omega_0$ it shows rather broad peaks shifted to larger values, although the resonance feature still remains throughout the different curves.

5 System beyond weak interactions

Up to now, we have only regarded weak particle-particle interactions, so regimes where the interaction term of the Hamiltonian is small compared to the kinetic energy and the potential. Now, we will extend our consideration and investigate the behaviour of an interaction term, which dominates the Hamiltonian. For this analysis we still use the Gross-Pitaevskii equation, even if we leave the limit of weak interactions. Consequently, the following results can maximal serve as plausibility statements, which need to be proven by a theory containing strong interactions.

To study the system's dependence on the strength of interaction, we examine the characteristics of the asymptotic current with respect to g. As can be seen in the plot of figure (5.1), there roughly exist two regimes. For $g \lesssim 2.45$ we observe a regular regime and for $g \gtrsim 2.45$ the system shows a non-regular characteristic. In the following we will explore, if the non-regular regime can be identified with a chaotic system. Therefore, it is necessary

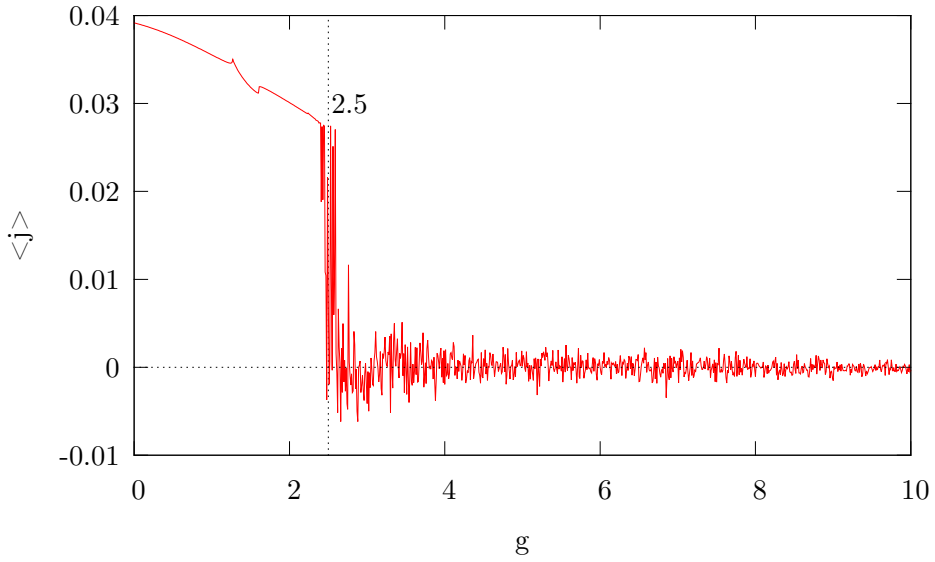

Figure 5.1: Asymptotic current plotted versus interaction strength g.
Parameters: $\omega = 2\pi\, 50\, \tau$, δ=1.0, $J_{0,1}$, $J_{0,2}$, V_0, δ_1, δ_2 and δ_V as before

to analyse the behaviour of the trajectories of the particles in phase space. In a regular system these trajectories should be lines. Since our system contains a large number N of particles and therefore also N degrees of freedom each for space and momentum as well as one global variable for the time, it is not an option to visualize the whole phase space trajectories. Instead, a common method is to do a Poincare map [36]. For this purpose, the set of the phase space trajectories are treated as a flow on a manifold M [37] of the dimension of the phase space, which is $2N+1$ as commented before. Furthermore, a global

cut is defined as a hyperplane S, which is a subspace of M with the properties, that (i) the flow is never tangential on S and (ii) every orbit has an infinite amount of intersections for $t \to \pm\infty$. It is then possible to define a Poincare map, which maps one intersection point of an orbit with a global cut $x \in S$ to the next one after the returning time $\tau(x)$ [37]. So for a periodic or quasi-periodic dynamic system, the intersection points form lines in the Poincare map. If one is able to find a map where these lines are closed, the system can certainly be regarded as regular. Vice versa non-closed lines do not imply a priori a chaotic behavior. If the trajectories in phase space are chaotic the intersection points are not related to each other, so that there arise clusters of points in the plot which cover limited areas. So the transition between a regular system to a chaotic systems contains intermediate states, where areas of points coexist with areas of smooth continuous lines [38]. With an increasing non-linear perturbation the point-covered areas expand.

In our case the information of the particle's degrees of freedom is inside the wave-function vector $|\psi(t)\rangle$ which is computed with the Runge-Kutta-method.

Our model is now described by the Hamiltonian and the current operator, given in equation (4.5) and (3.23). In matrix form these operators can be rewritten with (3.7) as

$$\hat{\mathcal{H}} = -\left(J_1(t) + J_2(t)\right)\hat{\sigma}_x + V(t)\hat{\sigma}_z + g|\psi|^2\mathbb{1} \qquad \text{and} \qquad \hat{j} = \left(J_1(t) - J_2(t)\right)\hat{\sigma}_y, \tag{5.1}$$

where $\hat{\sigma}_x$, $\hat{\sigma}_y$ and $\hat{\sigma}_z$ are the Pauli matrices

$$\sigma_x = \begin{pmatrix} 0 & 1 \\ 1 & 0 \end{pmatrix}, \qquad \sigma_y = \begin{pmatrix} 0 & -i \\ i & 0 \end{pmatrix}, \qquad \sigma_z = \begin{pmatrix} 1 & 0 \\ 0 & -1 \end{pmatrix}. \tag{5.2}$$

The Pauli matrices build an irreducible basis for the $SU(2)$ group. To obtain a Poincare map, the information of the wave function is mapped to a three dimensional space, using the expectation values of the Pauli matrices, given by

$$\left\langle \vec{\hat{\sigma}} \right\rangle_t = \begin{pmatrix} \langle \hat{\sigma}_x \rangle_t \\ \langle \hat{\sigma}_y \rangle_t \\ \langle \hat{\sigma}_z \rangle_t \end{pmatrix} = \begin{pmatrix} \langle \psi(t)|\hat{\sigma}_x|\psi(t)\rangle \\ \langle \psi(t)|\hat{\sigma}_y|\psi(t)\rangle \\ \langle \psi(t)|\hat{\sigma}_z|\psi(t)\rangle \end{pmatrix}, \tag{5.3}$$

as points in $\mathbb{R}^3$. This is a good choice because we are able to see directly the behaviour of the physical observables of the current, the potential and the hopping. An explicitly calculation shows that the distance of $\left\langle \vec{\hat{\sigma}} \right\rangle_t$ from the origin is equal to one for a normalized wave

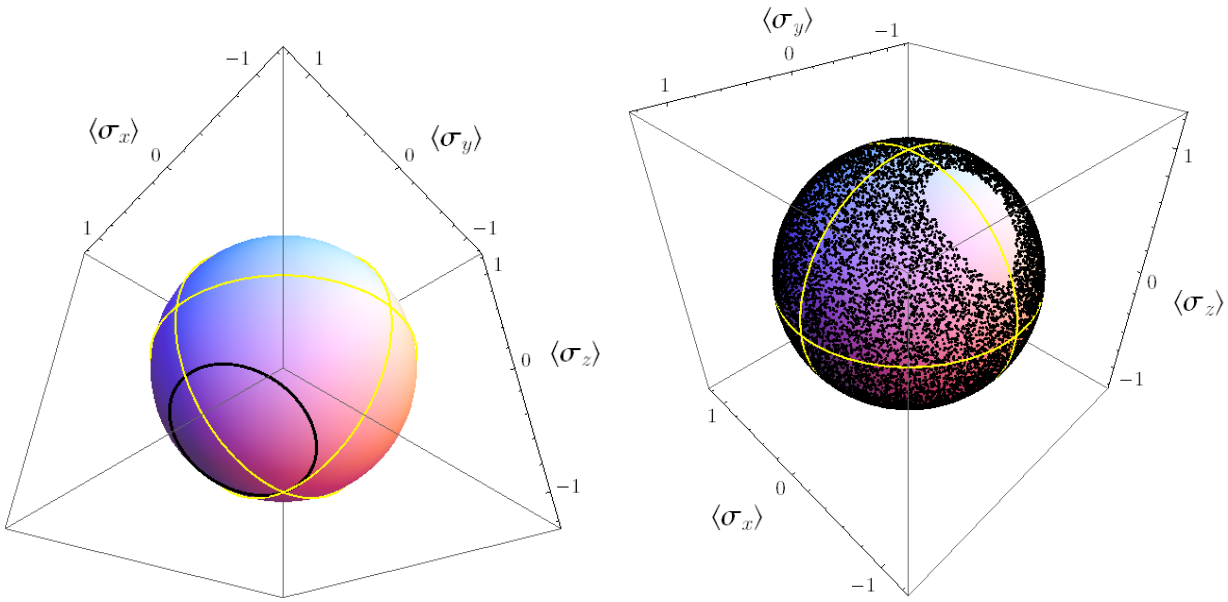

(a) regular regime (b) non-regular regime

Figure 5.2: Three-dimensional plot of the expectation values of the Pauli matrices, both for a regular regime with $g = 0$ and a highliy non-regular regime $g = 8$. the yellow lines guide the eye.

function. This is also valid, since the $\hat{\sigma}_i$ are unitary matrices and unitary transformations do not change the norm of a vector. Consequently, all points of $\left\langle \vec{\hat{\sigma}} \right\rangle_t$ are positioned on the surface of a unit sphere.

The plot in figure (5.2) shows the behaviour for two interaction strengths each representing one regime of figure (5.1), where (a) displays a regular regime with $g = 0$ and (b) a highly non-regular regime with $g = 8$. Every point on the sphere represents $\left\langle \vec{\hat{\sigma}} \right\rangle_t$ for different times t which are integer multiples of the period $T = \frac{\omega}{2\pi}$ of the driven system. This is assumed to be the returning time $\tau(x)$, where ω is the driving frequency. The total number of periods for these calculations was 30000 with the initial condition $|L, R\rangle = |0, 1\rangle$.

It can be seen for the non-interacting system, that the points form a closed loop on the spheric surface. As mentioned above this guarantees a regular system. For another view, covering the whole sphere in one image, the points are mapped to the spheric angles θ and

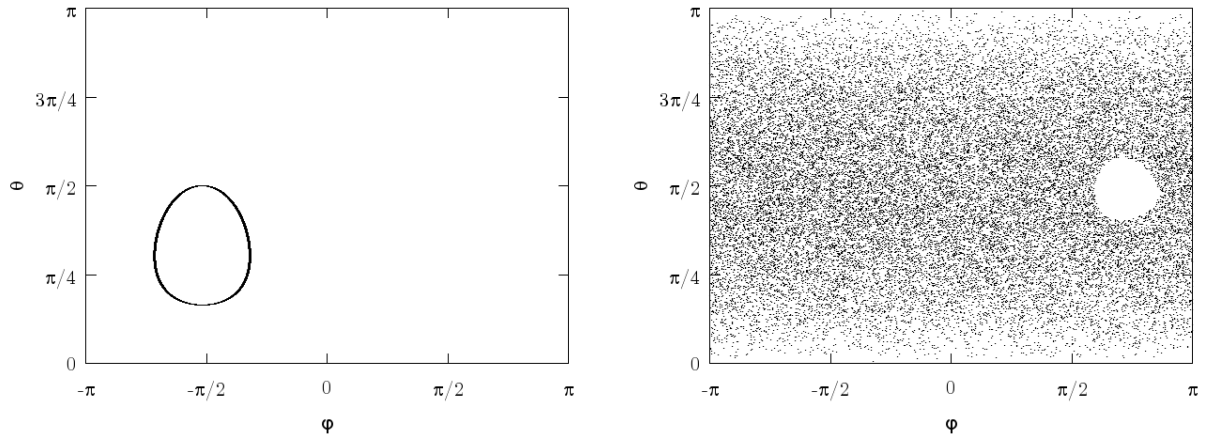

(a) regular regime

(b) non-regular regime

Figure 5.3: Transformation of the sphere in figure (5.2) to the spheric angles θ and φ by equation (5.4)

φ by the transformation

$$\begin{pmatrix} \langle\hat{\sigma}_x\rangle_t \\ \langle\hat{\sigma}_y\rangle_t \\ \langle\hat{\sigma}_z\rangle_t \end{pmatrix} \mapsto \begin{pmatrix} \theta \\ \varphi \end{pmatrix} = \begin{pmatrix} \arctan\left(\frac{\langle\sigma_z\rangle}{\langle\sigma_x\rangle}\right) \\ \arccos(\langle\sigma_y\rangle) \end{pmatrix}, \tag{5.4}$$

where the z-axis in the polar coordinate system has been laid in the direction of $(0,1,0)^T$. This is the direction of $\langle\hat{\sigma}_y\rangle_t$, which correlates with the current. The corresponding plots to figure (5.2) are shown in (5.3). The transformation does not conserve the form of the curves on the sphere, so the trajectory in (5.2 a) similar to a circle, appears modified in (5.3 a).

In contrast to the $g = 0$-model, the system does not show any structure under consideration of strong interaction (figure 5.2 b and 5.3). In fact, the expectation values do not depend on the driving properties of the system at all and therefore show no periodicity or smooth lines in the Poincare map. Nevertheless there is a region where no points are determined. The transition between these two regimes is very sharp, and is localized at a non-linearity of $g = 2.5$ witch coincides with the behaviour of the current in (5.1).

Until now we have chosen the same initial conditions $|L, R\rangle = |0, 1\rangle$ for both options. De facto every set-up starting in the area covered with points, reproduces the same trajectories as (5.2)(b) and (5.3)(b). The point of interest now is, to determine the arrangement of the

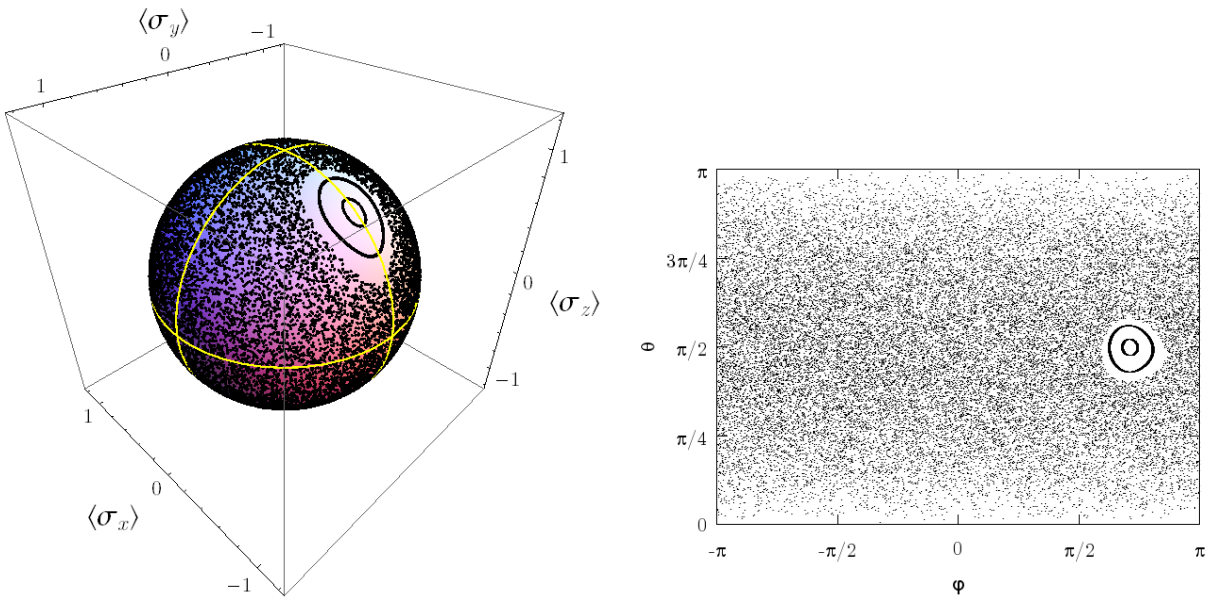

(a) spherical plot (b) mapped to the spheric angles

Figure 5.4: Analogous plots to 5.2 b and 5.3 b with the two additional initial conditions of equation (5.5)

points for initial conditions, which are located in the empty spaces of the strong-interaction images. So additionally to the data of the non-regular system before, in figure (5.4) the trajectories for

$$|L,R\rangle = |-0.67-0.67i, 0.24+0.19i\rangle \qquad \text{and} \qquad |L,R\rangle = |-0.67-0.67i, 0.29+0.13i\rangle \quad (5.5)$$

are included.

These initial conditions generate closed, non-crossing trajectories which are an indication for a regular system. Thus, even in the presence of very high particle-particle interaction, a system can evolve regularly in time. After all this matches qualitatively the expectations of two different areas in the Poincare plot. As a conclusion one can say, that the behaviour of the system, strongly depends on the choice of the initial conditions.

Once again we want to emphasize, that the obtained data was calculated with the Gross-Pitaevskii equation which was derived for the limiting case of weak-interaction, which is clearly left in the upper consideration with a non-linearity g of about eight times greater than the kinetic and potential energy. Nevertheless the obtained results are consistent to each other and can be used as a qualitative guidance.

6 Conclusions

We have considered the features of a periodically driven system and have obtained an asymptotic net-current originated in the quantum ratchet effect.

As a remarkable feauture of this quantity in the absence of interactions is that the only possibility to achieve a final net current is to break the time-reversal ($\varphi \neq n\pi$, $n \in \mathbb{N}_0$) and the spatial symmetry as discussed in Chapter 3. This result is in very good quantitative agreement with the numerical values of [5] as well as with the experimental data of [30] where the velocity of the unidirectional motion, respectively of the center of mass, vanishes for a restored temporal symmetry. Moreover as one can see in figure (4.1), the deviation of the weak-interacting ($g = 0.1$) behavior from the non-interacting system is insignificant compared to the absolute value of the current. This reproduces the conclusions of Ref. [5]. Furthermore the fact that the maximal particle transport occurs at $\varphi = \{\frac{\pi}{2}, \frac{3\pi}{2}\}$ reproduces the experimental findings of [30] qualitatively.

The computation of the resonance frequencies enables us to predict, with the knowledge of the other system parameters, the driving frequency which maximizes the current. However for temporal amplitudes similar to the constant values, the peaks at the position of resonance frequencies smear out and broaden enormously.

The study of a broad interval for the interactions yields the attendance of a regular and a non-regular regime which shows some chaotic properties. The transition between these two behaviours is found at a sharp value for the non-linearity g. Furthermore examining the Poincare cuts of the phase space one can find in the non-regular consideration empty areas where stable trajectories are observed if the initial conditions are chosen properly. This coincides with [39], where similar calculations are presented for a quantum treatment of a driven anharmonic oscillator. Our results therefore suggest, that the system for strong interactions becomes chaotic. To test this statement a theory beyond the mean-field approach is needed. To identify the non-regular regime undoubtedly a levelstatistics for the quasi-energies should be performed as it is done in Ref. [40].

Bibliography

[1] Courteille, Ph. ; Freeland, R. S. ; Heinzen, D. J. ; Abeelen, F. A. ; Verhaar, B. J.: Observation of a Feshbach Resonance in Cold Atom Scattering. In: *Phys. Rev. Lett.* 81 (1998), Jul, 69–72. http://dx.doi.org/10.1103/PhysRevLett.81.69. – DOI 10.1103/PhysRevLett.81.69

[2] R. Dean Astumian, Peter H.: Brownian Motors. In: *Physics Today* (2002)

[3] Jülicher, Frank ; Ajdari, Armand ; Prost, Jacques: Modeling molecular motors. In: *Rev. Mod. Phys.* 69 (1997), Oct, 1269–1282. http://dx.doi.org/10.1103/RevModPhys.69.1269. – DOI 10.1103/RevModPhys.69.1269

[4] Magnasco, Marcelo O.: Forced thermal ratchets. In: *Phys. Rev. Lett.* 71 (1993), Sep, 1477–1481. http://dx.doi.org/10.1103/PhysRevLett.71.1477. – DOI 10.1103/PhysRevLett.71.1477

[5] Creffield, C. E. ; Sols, F.: Coherent Ratchets in Driven Bose-Einstein Condensates. In: *Phys. Rev. Lett.* 103 (2009), Nov, 200601. http://dx.doi.org/10.1103/PhysRevLett.103.200601. – DOI 10.1103/PhysRevLett.103.200601

[6] Poletti, Dario ; Benenti, Giuliano ; Casati, Giulio ; Hänggi, Peter ; Li, Baowen: Steering Bose-Einstein Condensates despite Time Symmetry. In: *Phys. Rev. Lett.* 102 (2009), Apr, 130604. http://dx.doi.org/10.1103/PhysRevLett.102.130604. – DOI 10.1103/PhysRevLett.102.130604

[7] Ashcroft, Neil W. ; Mermin, David N.: *Festkörperphysik*. Oldenburg-Verlag München, Wien, 2001

[8] Gross, Rudolf ; Marx, Achim: *Festkörperphysik - Vorlesungskript zur Vorlesung im WS 2010/2011 und SS 2011*. http://www.wmi.badw-muenchen.de/teaching/Lecturenotes/index.html

[9] Shirley, Jon H.: Solution of the Schrödinger Equation with a Hamiltonian Periodic in Time. In: *Phys. Rev.* 138 (1965), May, B979–B987. http://dx.doi.org/10.1103/PhysRev.138.B979. – DOI 10.1103/PhysRev.138.B979

[10] Kohler, Sigmund: *The interplay of chaos and dissipation in driven quantum systems*, University of Augsburg, Diss., 1999

[11] Burmeister, Guido ; Maschke, Klaus: Influence of a time-periodic magnetic flux on interacting electrons in a one-dimensional loop. In: *Phys. Rev. B* 67 (2003), Apr,

165305. http://dx.doi.org/10.1103/PhysRevB.67.165305. – DOI 10.1103/PhysRevB.67.165305

[12] Phillips, William D.: Laser cooling and trapping of neutral atoms. In: *Rev. Mod. Phys Vol.10 No.3* (1998)

[13] Davis, K. B. ; Mewes, M. O. ; Andrews, M. R. ; Druten, N. J. ; Durfee, D. S. ; Kurn, D. M. ; Ketterle, W.: Bose-Einstein Condensation in a Gas of Sodium Atoms. In: *Phys. Rev. Lett.* 75 (1995), Nov, 3969–3973. http://dx.doi.org/10.1103/PhysRevLett.75.3969. – DOI 10.1103/PhysRevLett.75.3969

[14] Bloch, Immanuel: Exploring quantum matter with ultracold atoms in optical lattices. In: *Journal of Physics B: Atomic, Molecular and Optical Physics* 38 (2005), Nr. 9, S629. http://stacks.iop.org/0953-4075/38/i=9/a=013

[15] http://www.optical-lattice.com/

[16] http://www.physics.umd.edu/rgroups/amo/rolstonwebsite/bec.htm

[17] Collective Rayleigh scattering in a Bose Einstein condensate. (2008)

[18] Pickett, Warren E.: Second Quantization. http://yclept.ucdavis.edu/course/242/2Q_Fradkin.pdf

[19] Altland, Alexander ; Simons, By Ben D. (Hrsg.): *Condensed Matter Field Theory.* Cambridge University Press, 2010

[20] Landau, L.D. ; Lifshits, E.M. ; Pitaevskiĭ: *Statistical physics*

[21] Zwierlein, M. W. ; Stan, C. A. ; Schunck, C. H. ; Raupach, S. M. F. ; Gupta, S. ; Hadzibabic, Z. ; Ketterle, W.: Observation of Bose-Einstein Condensation of Molecules. In: *Phys. Rev. Lett.* 91 (2003), Dec, 250401. http://dx.doi.org/10.1103/PhysRevLett.91.250401. – DOI 10.1103/PhysRevLett.91.250401

[22] Franco Dalfovo, Lev P. P. ; Stringari, Sandro: Bose Einstein Condensates. (2005)

[23] Dalfovo, Franco ; Giorgini, Stefano ; Pitaevskii, Lev P. ; Stringari, Sandro: Theory of Bose-Einstein condensation in trapped gases. In: *Rev. Mod. Phys.* 71 (1999), Apr, 463–512. http://dx.doi.org/10.1103/RevModPhys.71.463. – DOI 10.1103/RevModPhys.71.463

[24] Kondov, Stanimir: Bose-Hubbard Model. (2008)

[25] Hoffmann, Alexander: *Bosonen im optischen Gitter*, Fachbereich Physik der Freien UniversitÂ¨at Berlin, Diplomarbeit, 2007

[26] Reimann, Peter ; Grifoni, Milena ; Hänggi, Peter: Quantum Ratchets. In: *Phys. Rev. Lett.* 79 (1997), Jul, 10–13. http://dx.doi.org/10.1103/PhysRevLett.79.10. – DOI 10.1103/PhysRevLett.79.10

[27] al., Salger et: Directed Transport of Atoms in a Hamiltonian Quantum Ratchet. In: *Science, Vol. 326 no. 5957 pp. 1241-1243* (2009)

[28] Magnasco, Marcelo O.: Forced thermal ratchets. In: *Phys. Rev. Lett.* 71 (1993), Sep, 1477–1481. http://dx.doi.org/10.1103/PhysRevLett.71.1477. – DOI 10.1103/PhysRevLett.71.1477

[29] Hänggi, Peter ; Marchesoni, Fabio: Artificial Brownian motors: Controlling transport on the nanoscale. In: *Rev. Mod. Phys.* 81 (2009), Mar, 387–442. http://dx.doi.org/10.1103/RevModPhys.81.387. – DOI 10.1103/RevModPhys.81.387

[30] Schiavoni, M. ; Sanchez-Palencia, L. ; Renzoni, F. ; Grynberg, G.: Phase Control of Directed Diffusion in a Symmetric Optical Lattice. In: *Phys. Rev. Lett.* 90 (2003), Mar, 094101. http://dx.doi.org/10.1103/PhysRevLett.90.094101. – DOI 10.1103/PhysRevLett.90.094101

[31] Hur, G. ; Creffield, C. E. ; Jones, P. H. ; Monteiro, T. S.: Chaotic quantum ratchets and filters with cold atoms in optical lattices: Analysis using Floquet states. In: *Phys. Rev. A* 72 (2005), Jul, 013403. http://dx.doi.org/10.1103/PhysRevA.72.013403. – DOI 10.1103/PhysRevA.72.013403

[32] al., H. L.: Experimental Tunneling Ratchets. In: *Science* (1999)

[33] NUMERICAL RECIPES IN C: THE ART OF SCIENTIFIC COMPUTING. (1988-1992)

[34] Shampine, Lawrence F.: Interpolation for Runge-Kutta Methods. In: *SIAM Journal on Numerical Analysis* 22 (1985), Nr. 5, pp. 1014-1027. http://www.jstor.org/stable/2157411. – ISSN 00361429

[35] *Theoretische Physik 2, Nichtrelativistische Quantentheorie*. Springer Berlin Heidelberg New York, 1999

[36] *Introduction to Applied Nonlinear Dynamical Systems and Chaos*. Springer-Verlag New York, 2003

[37] *Einführung in Dynamische Systeme*. 2010 http://www.math.uni-hamburg.de/home/gunesch/Vorlesung/SoSe2010/Vorl_Einf_Dyn_Sys/Skript/Gunesch-EinfDynSys-Skript.pdf

[38] *Theoretische Physik: Mechanik*. Elsevier GmbH, Spektrum Akademischer Verlag, 2006

[39] Lin, W. A. ; Ballentine, L. E.: Quantum tunneling and chaos in a driven anharmonic oscillator. In: *Phys. Rev. Lett.* 65 (1990), Dec, 2927–2930. http://dx.doi.org/10.1103/PhysRevLett.65.2927. – DOI 10.1103/PhysRevLett.65.2927

[40] H. Frahm, H.J. M.: Levelstatistics and Stochasticity in a Driven Quantum System. In: *Z. Phys. B - Condensed Matter* (1986)

[41] SIKRI, A K. ; NARCHAL, M L.: Floquet states of a periodically kicked particle. In: *Pramana - journal of physics* 40 (1993), April, Nr. 4, S. 267–272

[42] Olbrich, P. ; Karch, J. ; Ivchenko, E. L. ; Kamann, J. ; März, B. ; Fehrenbacher, M. ; Weiss, D. ; Ganichev, S. D.: Classical ratchet effects in heterostructures with a lateral periodic potential. In: *Phys. Rev. B* 83 (2011), Apr, 165320. http://dx.doi.org/10.1103/PhysRevB.83.165320. – DOI 10.1103/PhysRevB.83.165320

Acknowledgement

First of all I want to thank Prof. Achim Rosch for suggesting to me the topic of quantum ratchets and therewith gave me the chance to work in an interesting and dynamical research area. I also appreciated the effort and interest regarding the thesis in several opportunities.

I further want to express special thanks to Dr. Karen Rodriguez for spending so much time on discussing and explaining difficult mathematical and physical concepts in a very understandable and motivating way. Thanks also for the patience and the work in correcting the thesis and answering questions concerning physical as well as language issues.

Further I want to thank my parents for the financial aid, which allowed me to focus solely on the studying of such an intensive and interesting field of study as physics.

Last but not least, I want to thank my family, friends and fellow student for every other kind of support.

Declaration

Herewith I affirm that I have written this thesis on my own. I did not enlist unlawful assistance of someone else. Cited sources of literature are perceptibly marked and listed at the end of this thesis. The work was not submitted previously in same or similar form to another examination committee and was not yet published.

_____

Stefan Wolff, Cologne, April 11, 2012